ISSN 2278-2540 | DOI: 10.51583/IJLTEMAS | Volume XIV, Issue XII, December 2025

# Caputo-Fabrizio Fractional Order Derivative Mathematical Modeling and Optimal Control, Cost-Effectiveness Analysis of Diphtheria Transmission Dynamics in Nigeria

**Musa. Abdullahi[1], Abdullahi M. Auwal[2*,] and Umar Abbas Faruk [3]**

**[1,3]Mathematics and Statistics Department, Gombe State Polytechnic, Bajoga**

**[2] Mathematics and Statistics Department, Federal Polytechnic, Bauchi**

**DOI : https://doi.org/10.51583/IJLTEMAS.2025.1412000054**

**Received: 18 December 2025; Accepted: 25 December 2025; Published: 03 January 2026**

## ABSTRACT

Diphtheria, a potentially fatal vaccine-preventable disease caused by *Corynebacterium diphtheriae*, has seen a resurgence in several regions, including sub-Saharan Africa. This study presents a comprehensive mathematical model for diphtheria transmission dynamics that incorporates environmental bacterial persistence, public awareness campaigns, and vaccine hesitancy. The model subdivides the human population into epidemiologically relevant classes, including susceptible, exposed, symptomatic infectious, asymptomatic infectious, vaccinated, and hesitant individuals, with an additional compartment representing environmental bacterial load. Analytical results establish the model's positivity, boundedness, and stability properties, with the basic reproduction number ($\mathcal{R}_0$) derived to determine disease threshold conditions. A global sensitivity analysis using the Partial Rank Correlation Coefficient (PRCC) identified the transmission rate ($\beta_1$), exposure progression rate ($\sigma$), and vaccination rate ($\delta$) as the most influential parameters affecting $\mathcal{R}_0$. The optimal control analysis, formulated via Pontryagin's Maximum Principle, evaluated time-dependent interventions representing vaccination, treatment, and public enlightenment efforts. Numerical simulations using parameterized incidence data from Bauchi State, Northeast Nigeria, revealed that combined control strategies significantly reduce infection prevalence and environmental contamination compared to single interventions. The cost-effectiveness analysis (CEA) demonstrated that the combined vaccination and public enlightenment campaign strategy produced the lowest Incremental Cost-Effectiveness Ratio (ICER) and was classified as "very cost-effective" according to WHO-CHOICE thresholds. The findings underscore that effective control requires a multi-pronged, dynamically-adapted strategy targeting all transmission pathways. High vaccination coverage remains the cornerstone, but its impact is significantly amplified when synergistically combined with public health campaigns and environmental decontamination. The results offer evidence-based, cost-effective guidance for public health policymakers to design efficient diphtheria outbreak response and elimination programs. Moreover, numerical solutions obtained for different fractional orders highlight the Caputo-Fabrizio fractional derivative's capability to simulate memory effects, thereby offering a more nuanced representation of the real-life problem under study.

**Keywords:** Diphtheria, Mathematical Modelling, Caputo-Fabrizio fractional derivative, Basic Reproduction Number, Global Sensitivity Analysis, Vaccination, Public Health Campaigns.

## INTRODUCTION

Corynebacterium diphtheriae, the causative agent of the potentially fatal infectious illness diphtheria, produces a toxin that can cause serious respiratory and systemic complications [1]. Although diphtheria is vaccine-preventable, the disease has re-emerged as a significant public health concern in Nigeria, particularly in the Northeast region. This resurgence, despite the availability of effective vaccines, underscores persistent gaps in immunization coverage, public health awareness, and healthcare delivery systems. Transmission occurs primarily through respiratory droplets or contact with infected surfaces. Symptoms typically appear 2–5 days post-infection and range from sore throat and fever to severe complications such as airway obstruction,

ISSN 2278-2540 | DOI: 10.51583/IJLTEMAS | Volume XIV, Issue XII, December 2025

myocarditis, and neuropathy. In Nigeria, the burden is disproportionately high among children aged 2–14 years, who constitute the majority of recent cases.

The symptoms range from mild to severe. At the mild stage, symptoms include a sore throat and fever; at the severe stage, symptoms include difficulty breathing and swallowing, as well as a barking cough. Inflammation and damage of the heart muscles, nerves, and kidney-related problems can also occur [45] and [24]. It is, therefore, advisable that infected persons seek treatment to help prevent serious complications [31]. Diphtheria is treated with antibiotics and diphtheria antitoxin, which kill the bacteria and prevent them from destroying body tissues [11]. Diphtheria can be transmitted among humans via contact with respiratory droplets, such as coughing and sneezing, or through indirect contact with contaminated clothing and objects ([11, 24, 45]). [3] states that an asymptomatic infected person can infect others for up to four weeks. Timely vaccination with the prescribed vaccines is the best defense against diphtheria ([11, 31, 8]). According to [24], children and adolescents should receive three booster doses of the diphtheria toxoid-containing vaccination [45]. Consequently, [24] recommends educating parents on the advantages of routine immunization to prevent diphtheria. Adults and newborns can also receive vaccinations. Over time, the effectiveness of the vaccines decreases; for roughly ten years, they provided 97 out of 100 protection against diphtheria ([11, 24]). Wearing personal protective equipment (PPE), which is disposed of right away after leaving patients' rooms, protects medical personnel against the disease [45].

The increasing prevalence of diphtheria in Nigeria is highlighted by recent statistics from the Nigeria Centre for Disease Control [32]. Four states, Kano (107 instances), Yobe (2), Lagos (1), and Osun (1) reported 111 confirmed cases and 22 fatalities between December 1, 2022, and the third week of January, 2023. For confirmed and probable cases, the case fatality rate (CFR) was 19.8%. Children between the ages of 2 and 14 accounted for a substantial majority of cases (91.9%). Remarkably, only 10.8% of these verified cases had been fully immunized with a vaccine containing diphtheria toxin [11]. By April 2023, the outbreak had intensified. Confirmed cases rose to 672 across seven states, with 491 cases affecting children aged 2–14 years. Out of these, only 144 were fully vaccinated. Factors contributing to the rapid spread include low immunization coverage, limited access to healthcare, poor socioeconomic conditions, low education levels, particularly in rural areas, and delayed clinical recognition of the disease [45].

In June 2023, reported cases increased further to 836, with over 70% involving children within the 2–14 age group. By 31 July 2023, the outbreak had expanded significantly to 1,534 confirmed cases across several states, including Kano, Lagos, Yobe, Katsina, Kaduna, Bauchi, the Federal Capital Territory (FCT), Niger, Gombe, Jigawa, Cross River, and Osun. The death toll rose to 137, but the CFR declined to 8.9%, likely due to improved availability and use of diphtheria antitoxin and antibiotics [31]. However, the aforementioned diphtheria infection outbreak significantly exceeds the last major diphtheria event in Nigeria, which occurred from February to November 2011 in Kimba village and surrounding settlements in Borno State. Only 98 cases were recorded, with a CFR of 21.4%, mostly affecting children under the age of 10. Notably, none of the affected individuals in that outbreak had received prior vaccination against diphtheria [24]. Despite national immunization programs, including the pentavalent DTP vaccine, coverage remains insufficient. For instance, the third-dose coverage (DTP3) declined from 86% in 2019 to 81% in 2021, with some states reporting coverage as low as 20%, far below the herd immunity threshold of 75–80%. Barriers to uptake include vaccine hesitancy, misinformation, maternal education levels, household decision-making dynamics, vaccine stockouts, and healthcare workforce shortages [1].

Several epidemiological models of diphtheria exist in the literature. For instance, [7] used mathematical modelling of antibody decay to estimate seroprotection rates 10 years post-vaccination. [15] developed an age-structured model of diphtheria transmission, employing non-linear differential equations to assess the global stability of the system. Similarly, [46] utilized a next-generation matrix approach for global stability analysis and parameter estimation. Studies by [19] explored quarantine’s impact on diphtheria dynamics, highlighting the role of early detection in controlling the spread. Furthermore, [47] developed an optimal control model to determine cost-effective strategies for reducing transmission, incorporating both cost and vaccination effectiveness. Other works, such as [29], emphasize vaccination’s impact on outbreak dynamics through simulation-based modeling and sensitivity analysis. [20] Conducted a sensitivity analysis of diphtheria

ISSN 2278-2540 | DOI: 10.51583/IJLTEMAS | Volume XIV, Issue XII, December 2025

transmission parameters, identifying key areas for intervention. [38] analyzed data from Nigeria's Isin Local Government Area to assess gender effects on transmission, while [19] examined vaccine efficacy using stability analysis within the SEIR model framework. Finally, [21] provided a dynamical analysis of diphtheria with natural immunity rates, exploring stability under different equilibrium conditions.

Mathematical modeling serves as a powerful tool for understanding infectious disease dynamics and guiding control strategies [34]. However, existing models often fail to account for Nigeria-specific challenges such as regional heterogeneity, behavioral dynamics, environmental factors, and healthcare system constraints. These limitations hinder the development of effective, data-driven interventions tailored to local contexts.

In another development, Fractional calculus has emerged as a vital framework for modelling complex physical systems that exhibit memory and nonlocal effects, phenomena that are challenging to capture with classical integer-order derivatives [13]. A significant limitation of early fractional operators was the singularity in their kernels at the termination point of the definition interval. This has spurred the development of numerous non-singular kernel definitions in recent literature.

The primary distinction among fractional derivatives lies in their kernels, which can be tailored to specific applications. Key developments include the singular power-law kernel of the Caputo derivative [13], the non-singular exponential decay kernel of the Caputo-Fabrizio (CF) derivative [9], and the non-singular Mittag-Leffler law kernel of the Atangana-Baleanu (AB) derivative [5]. Comparative studies have highlighted the practical advantages of these new operators. For instance, in modeling chaotic systems, the CF derivative was found to produce less noise than the power-law-based Riemann-Liouville derivative [5]. The CF derivative, in particular, was explicitly designed to model memory effects without singularities, and its corresponding fractional integral has been rigorously defined [27].

Leveraging these advanced mathematical tools, this study addresses some gaps by developing a novel deterministic integer- and non-integer-order model of diphtheria transmission that integrates regional demographic variation, vaccine hesitancy, environmental influences, and public health campaign dynamics. Using incidence data from the Specialist Hospital, Bauchi State Ministry of Health, for the period from January to December 2023, we conduct a sensitivity analysis to identify key parameters driving disease persistence. We also apply optimal control theory to evaluate cost-effective intervention strategies suited to Nigeria's resource-constrained healthcare environment.

**The description of the model**

The proposed model is of the SEIR-compartment type, and to investigate the transmission of diphtheria, we include vaccinated individuals, hesitant individuals, and the concentration of germs in the environment in the region τ compartments. Thus, the entire population at time t, is split up into eight distinct compartments, with those at risk of contracting the diphtheria infection, susceptible individuals $S_\tau(t)$, Humans who are exposed to the virus but not yet infectious, exposed individuals $E_\tau(t)$, Asymptomatic individuals are capable of transmitting the virus, but those not exhibiting any symptoms associated with the disease $A_\tau(t)$, infected individuals capable of transmitting the virus $I_\tau(t)$, those who recovered from the infection $R_\tau(t)$, humans who received vaccinations $V_\tau(t)$, and those who are uncertain, skeptical, or resistant to vaccination, often due to the lack of information/campaign, fear of side effects, and personal or philosophical beliefs, are hesitant individuals $H_\tau(t)$ and the Concentration of the bacteria in the environment $W_\tau$.

Then we assume the following:

i. The population (group of persons) being studied is homogeneously mixed.

ii. The yearly outbreaks of diphtheria in Africa (Nigeria) over a comparatively long period of time provide some insight into the demographic process due to new births, migration, and deaths (natural or from diseases).

iii. People may still be at risk of getting diphtheria even after receiving their first dose of the vaccine.

ISSN 2278-2540 | DOI: 10.51583/IJLTEMAS | Volume XIV, Issue XII, December 2025

iv. People who have recovered quickly from treatment or have not experienced any symptoms may eventually lose their immunity and become vulnerable to diphtheria.

Thus, the governing equations are presented in equation (1).

$$\frac{dS_\tau}{dt} = \Pi - \lambda_\tau S_\tau + \omega V_\tau + \pi H_\tau \ - (\delta + \xi + \mu)S_\tau$$

$$\frac{dE_\tau}{dt} = \lambda_\tau S_\tau - (\sigma + \mu)E_\tau$$

$$\frac{dI_\tau}{dt} = \sigma\varsigma E_\tau - (\gamma_1 + \phi_1 + \mu)I_\tau$$

$$\frac{dA_\tau}{dt} = \sigma(1-\varsigma)E_\tau - (\gamma_2 + \phi_2 + \mu)A_\tau$$

$$\frac{dR_\tau}{dt} = \gamma_1 I_\tau + \gamma_2 A_\tau - \mu R_\tau \qquad (1)$$

$$\frac{dV_\tau}{dt} = \delta S_\tau - (\omega + \mu)V_\tau$$

$$\frac{dH_\tau}{dt} = \xi S_\tau - (\pi + \mu)H_\tau$$

$$\frac{dW_\tau}{dt} = \varphi_1 I_\tau + \varphi_2 A_\tau - \vartheta W_\tau$$

$$\lambda_\tau = (1 - C\varepsilon)\left[\frac{\beta_1(I_\tau + \theta A_\tau)}{N_\tau} + \frac{\beta_2 W_\tau}{\kappa + W_\tau}\right], \qquad 0 \le C\varepsilon \le 1 \qquad (2)$$

Where $\beta_1$ is the transmission rate. Moreover, it is believed that the free viruses in contaminated environments exhibit a Hill function or logistic-dose response curve. $\frac{W_\tau}{\kappa + W_\tau}$ , where $\kappa$ is the concentration of the pathogen in the environment, which accelerates the possibility of triggering the disease transmission, and $\beta_2$ stands as the human exposure rate to free viruses in the surrounding environment.

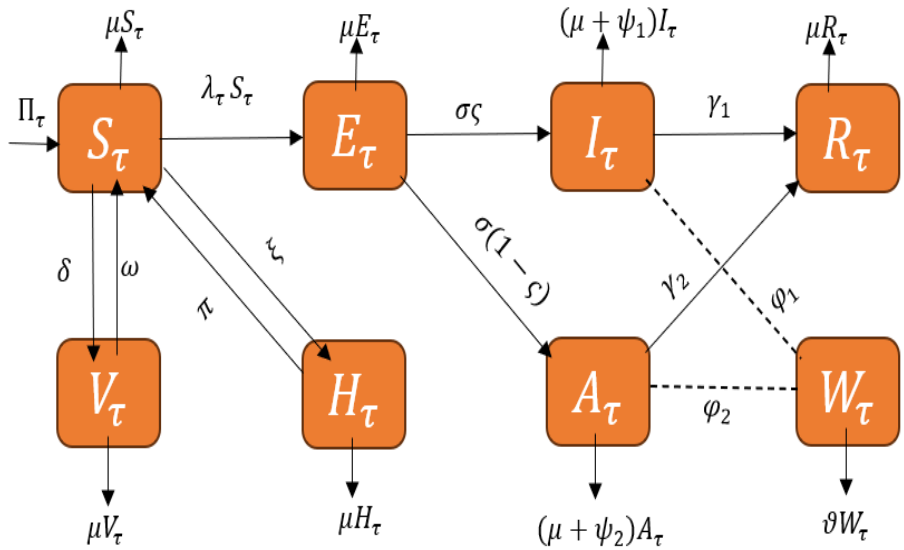


**Figure 1: The model's schematic flow diagram (1)**

ISSN 2278-2540 | DOI: 10.51583/IJLTEMAS | Volume XIV, Issue XII, December 2025

**Description of the state variables and the parameters of the flow chart model**

| Variable | Description |
|---|---|
| $S_\tau(t)$ | Susceptible individuals in the region $\tau$ |
| $E_\tau(t)$ | Exposed individuals in the region $\tau$ |
| $I_\tau(t)$ | Symptomatic infected individuals in the region $\tau$ |
| $A_\tau(t)$ | Asymptomatic infected individuals in the region $\tau$ |
| $R_\tau(t)$ | Recovery individuals in the region $\tau$ |
| $V_\tau(t)$ | Vaccinated individuals in the region $\tau$ |
| $H_\tau(t)$ | Hesitant individuals in the region $\tau$ |
| $W_\tau(t)$ | Concentration of the bacteria in the environment in the region $\tau$ |

**Table 1. The state variables of the flow chart model system**

| Parameters | Descriptions |
|---|---|
| $\Pi$ | Recruitment/birth rate into the Susceptible population |
| $\mu$ | The natural death rate |
| $\sigma$ | The rate at which exposed individuals become infectious |
| $\theta\epsilon(0,1)$ | Modification parameter for the infectiousness of asymptomatic individuals relative to symptomatic one |
| $\delta$ | Vaccination rate of Susceptible individuals |
| $\gamma_1, \gamma_2$ | Recovery rates for symptomatic and asymptomatic individuals, respectively |
| $\phi_1, \phi_2$ | Disease-induced mortality rate for symptomatic and asymptomatic individuals, respectively |
| $\omega$ | Waning immunity rate (Loss of vaccine protection) |
| $\xi$ | The rate at which Susceptible individuals become hesitant, |
| $\pi$ | The rate at which public campaigns convert hesitant individuals back to Susceptible |
| $\beta_1$ | The transmission in the region $\tau$ |
| $\varsigma\epsilon(0,1)$ | Proportion of exposed individuals who become symptomatic |
| $C$ | Intensity of the Public Enlightenment Campaign |

ISSN 2278-2540 | DOI: 10.51583/IJLTEMAS | Volume XIV, Issue XII, December 2025

| | |
|---|---|
| $\epsilon$ | Efficacy/compliance rate of the public enlightenment campaign |
| $\varphi_1, \varphi_2$ | The rate of bacterial shedding into the environment by $I_\tau$ $and$ $A_\tau$, respectively |
| $\vartheta$ | Bacteria decay rate in the environment /pathogens decay rate |

**Table 2. The parameters of the flow chart model system**

**Analysis of the model**

**Mathematical well-posedness**

**Theorem 1:** The domain $\Omega_\tau$ of the model system (1), which is defined as

$\Omega_\tau = \Omega_h \times \Omega_e$, Where $\Omega_h = \{(S_\tau, E_\tau, I_\tau, A_\tau, R_\tau, V_\tau, H_\tau, W_\tau) \in \mathbb{R}_+^7 : 0 < N_\tau \leq \frac{\Pi}{\mu}\}$ and

$\Omega_e = \{(W_\tau) \in \mathbb{R}_+^1 : \ W_\tau \geq 0\}$, are an invariant positive attractor of a subset for the human population and the contamination environment, respectively.

**Proof.** We sum the human population equations of model (1) to obtain

$$\frac{dN_\tau(t)}{dt} = \Pi - \mu N_\tau(t) - \phi_1 I_\tau - \phi_2 A_\tau \tag{3}$$

Since $\phi_1 I_\tau \geq 0$ $and$ $\phi_2 A_\tau \geq 0$, Upon simplification, we have the inequality $\frac{dN_\tau(t)}{dt} = \Pi - \mu N_\tau(t)$

$$\frac{dN_\tau(t)}{dt} \leq \Pi - \mu N_\tau(t)$$

Which gives

$$N_\tau(t) \leq \frac{\Pi}{\mu} + \left[N_\tau(0) - \frac{\Pi}{\mu}\right] e^{-\mu t}$$

It follows that if $t$ tends to zero, then $N_\tau(t)$ approaches $N_\tau(0)$, which implies that $\frac{\Pi}{\mu}$ is the upper bound of $N_\tau(t)$ and $N_\tau(t) \to \frac{\Pi}{\mu}$ provided $t$ tends to $+\infty$.

$\limsup_{t\to\infty} N_\tau(t) \leq \frac{\Pi}{\mu}$. Therefore, the total human population is always bounded above by $\Pi/\mu$.

Similarly, from the pathogen equation:

$$\frac{dW_\tau}{dt} = \varphi_1 I_\tau + \varphi_2 A_\tau - \vartheta W_\tau \tag{4}$$

Since $I_\tau \leq N_\tau \leq \Pi/\mu$ and $A_\tau \leq N_\tau \leq \Pi/\mu$, we can define an upper bound for the shedding rate:

$$\varphi_1 I_\tau + \varphi_2 A_\tau \leq \varphi_{max} \frac{\Pi}{\mu}$$

where $\varphi_{max} = \max(\varphi_1, \varphi_2)$. Thus,

$$\frac{dW_\tau}{dt} \leq \varphi_{max} \frac{\Pi}{\mu} - \vartheta W_\tau$$

ISSN 2278-2540 | DOI: 10.51583/IJLTEMAS | Volume XIV, Issue XII, December 2025

By the comparison theorem. The solution is bounded by:

$$W_\tau(t) \le W_\tau(0)e^{-\vartheta t} + \frac{\varphi_{max}\Pi}{\mu\vartheta}(1 - e^{-\vartheta t})$$

Taking the limit as $t \to \infty$:

$$\limsup_{t\to\infty} W_\tau(t) \le \frac{\varphi_{max}\Pi}{\mu\vartheta}$$

Therefore, the pathogen concentration is also uniformly bounded.

Since all state variables are non-negative and bounded above, the feasible region $\Omega_\tau$ is positively invariant and attracting. Any solution starting in $\Omega_\tau$ remains there for all $t > 0$. Hence, model (1) is well-posed and biologically meaningful.

**Diphtheria Disease-free equilibrium and Stability result**

The DDFE is the state in which no infection exists in the population in Model 1.

Therefore, the Diphtheria Disease-free equilibrium of the model (1) is obtained by setting the right-hand side of the model system (1) equal to zero at the steady state $\left(\widetilde{S_\tau} = \widetilde{E_\tau} = \widetilde{I_\tau} = \widetilde{R_\tau} = \widetilde{V_\tau} = \widetilde{H_\tau} = 0\right)$, and solving the resultant algebraic equations simultaneously

Then, the DDFE is characterized by

$$\tilde{\Sigma} = \left(\widetilde{S_\tau}, \widetilde{E_\tau}, \widetilde{I_\tau}, \widetilde{A_\tau}, \widetilde{R_\tau}, \widetilde{V_\tau}, \widetilde{H_\tau}, \widetilde{W_\tau}\right) = \left(\widetilde{S_\tau}, 0,0,0,0, \widetilde{V_\tau}, \widetilde{H_\tau}, 0\right) \quad (5)$$

Where $\widetilde{S_\tau} = \frac{\Pi(\pi+\mu)}{(\delta+\xi+\mu)(\pi+\mu)-\xi\pi}, \widetilde{V_\tau} = \frac{\delta}{\omega+\mu}\widetilde{S_\tau}, and\ \widetilde{H_\tau} = \frac{\xi}{\pi+\mu}\widetilde{S_\tau}$

**Basic reproduction number $\mathcal{R}_0$**

A threshold parameter known as the basic reproduction number, denoted by $\mathcal{R}_0$ , is needed to examine the linear stability of this equilibrium point. The technique described in [39] can be used to determine such a threshold parameter. We have the following matrices for the new infection terms and the transition terms, respectively, using the matrix notation provided by these authors.

$$\mathcal{F} = \begin{pmatrix} 0 & \beta_1(1-C\varepsilon)\frac{\widetilde{S_\tau}}{\widetilde{N_\tau}} & \beta_1\theta(1-C\varepsilon)\frac{\widetilde{S_\tau}}{\widetilde{N_\tau}} & \beta_2(1-C\varepsilon) \\ 0 & 0 & 0 & 0 \\ 0 & 0 & 0 & 0 \\ 0 & 0 & 0 & \end{pmatrix},$$

$$\nu = \begin{pmatrix} (\sigma+\mu) & 0 & 0 & 0) \\ -\sigma\varsigma & (\gamma_1+\phi_1+\mu) & 0 & 0 \\ -\sigma(1-\varsigma) & 0 & (\gamma_2+\phi_2+\mu) & 0 \\ 0 & -\varphi_1 & -\varphi_2 & \vartheta \end{pmatrix}$$

It follows that we can compute the basic reproduction number $\mathcal{R}_0$ with $\mathcal{F}$ (new infections) and $\nu$ (transitions) as follows:

$\mathcal{R}_0 = \rho(FV^{-1})$, the spectral radius of the next-generation matrix. Thus,

$$\mathcal{R}_0 = (1-C\varepsilon)\frac{\widetilde{S_\tau}}{\widetilde{N_\tau}} \cdot \frac{\sigma}{\sigma+\mu}\left[\frac{\beta_1\varsigma}{\gamma_1+\phi_1+\mu} + \frac{\beta_1\theta(1-\varsigma)}{\gamma_2+\phi_2+\mu} + \frac{\beta_2}{\vartheta}\left(\frac{\varphi_1\varsigma}{\gamma_1+\phi_1+\mu}\right) + \frac{\varphi_2(1-\varsigma)}{\gamma_2+\phi_2+\mu}\right] \quad (6)$$

ISSN 2278-2540 | DOI: 10.51583/IJLTEMAS | Volume XIV, Issue XII, December 2025

Where $\mathcal{R}_0 = \mathcal{R}_{I_\tau} + \mathcal{R}_{A_\tau} + \mathcal{R}_{W_\tau}$

With

$$\mathcal{R}_{I_\tau} = \frac{\beta_1(1-C\varepsilon)\widetilde{S_\tau}}{N_\tau} \times \frac{\sigma\varsigma}{(\sigma+\mu)} \times \frac{1}{(\gamma_1+\phi_1+\mu)},$$

$$\mathcal{R}_{A_\tau} = \frac{\beta_1\theta(1-C\varepsilon)\widetilde{S_\tau}}{N_\tau} \times \frac{\sigma(1-\varsigma)}{(\sigma+\mu)} \times \frac{1}{(\gamma_2+\phi_2+\mu)},$$

$$\mathcal{R}_{W_\tau} = \frac{\beta_2(1-C\varepsilon)\widetilde{S_\tau}}{N_\tau} \frac{\sigma}{\vartheta(\sigma+\mu)} \left( \frac{\varphi_1\varsigma}{(\gamma_1+\phi_1+\mu)} + \frac{\varphi_2(1-\varsigma)}{(\gamma_2+\phi_2+\mu)} \right).$$

And

$\mathcal{R}_{I_\tau}, \mathcal{R}_{A_\tau}$and $\mathcal{R}_{W_\tau}$ is the number of secondary cases generated through direct transmission from symptomatic individuals ($I_\tau$), asymptomatic individuals ($A_\tau$), and indirect transmission from the contaminated environment ($W_\tau$), respectively.

**Local Stability of the Diphtheria Disease-free Equilibrium** (**DDFE**)

**Theorem 2 (Local Asymptotic Stability)**

The diphtheria disease-free equilibrium of the model (1) is locally asymptotically stable if $\mathcal{R}_0 < 1$and is unstable if $\mathcal{R}_0 > 1$.

**Proof**

Linearize the full system about the DFE. The Jacobian has the block form

$$J(\tilde{\Sigma}) = \begin{pmatrix} J_1 & J_2 \\ 0 & J_3 \end{pmatrix},$$

where the top-left block $J_1$ corresponds to an uninfected subsystem $(S_\tau, V_\tau, H_\tau, R_\tau)$ and the bottom-right block $J_3$ is the infection subsystem Jacobian (the $4 \times 4$block associated with $(E_\tau, I_\tau, A_\tau, W_\tau)$ this is the same block that produces $\mathcal{F}$and $\nu$ upon decomposition). Because $J(\tilde{\Sigma})$ is block lower-triangular, its spectrum equals the union of the spectra of $J_1$ and $J_3$. Under biologically realistic parameter values, the uninfected block $J_1$ has eigenvalues with negative real parts (simple linear algebra: diagonal dominant negative terms because of mortality and conversion rates), so local stability reduces to the spectrum of the infection block $J_3$.

[39] show that the sign of the real parts of the eigenvalues of $J_3$ is determined by $\rho(K) = \mathcal{R}_0$: all eigenvalues of $J_3$ have negative real parts iff $\mathcal{R}_0 < 1$. Hence $\tilde{\Sigma}$ is locally asymptotically stable when $\mathcal{R}_0 < 1$and unstable when $\mathcal{R}_0 > 1$.

**Global Asymptotic Stability of the disease-free equilibrium**

**Theorem 3 (Global Asymptotic Stability)**

Consider the model system (1) with initial conditions in the biologically feasible region $\Omega_\tau$. The Disease-Free Equilibrium $\tilde{\Sigma}$, is globally asymptotically stable in $\Omega_\tau$ if $\mathcal{R}_0 \leq 1$.

**Proof.** To prove the global stability of $\tilde{\Sigma}$, we employ the method of Lyapunov functions, a powerful technique in stability theory for dynamical systems (Khalil, 2002). We construct a candidate Lyapunov function $L$ for the infected compartments.

Let us define the following Lyapunov function:

ISSN 2278-2540 | DOI: 10.51583/IJLTEMAS | Volume XIV, Issue XII, December 2025

$$L(E_\tau, I_\tau, A_\tau, W_\tau) = E_\tau + \frac{K\beta_1}{k_2} I_\tau + \frac{K\beta_1\theta}{k_3} A_\tau + \frac{K\beta_2}{\vartheta} W_\tau,$$

where $K = (1 - C\varepsilon)\frac{\widetilde{S_\tau}}{\widetilde{N_\tau}} k_2 = (\gamma_1 + \phi_1 + \mu)$, and $k_3 = (\gamma_2 + \phi_2 + \mu)$.

The time derivative of $L$ along the trajectories of the system is given by:

$$\frac{dL}{dt} = \frac{dE_\tau}{dt} + \frac{K\beta_1}{k_2}\frac{dI_\tau}{dt} + \frac{K\beta_1\theta}{k_3}\frac{dA_\tau}{dt} + \frac{K\beta_2}{\vartheta}\frac{dW_\tau}{dt} \quad (7)$$

Substituting the required model equations into the $(7)$ we have:

$$\frac{dL}{dt} = [\lambda_\tau S_\tau - k_1 E_\tau] + \frac{K\beta_1}{k_2}[\sigma\varsigma E_\tau - k_2 I_\tau] + \frac{K\beta_1\theta}{k_3}[\sigma(1-\varsigma)E_\tau - k_3 A_\tau] +$$

$$\frac{K\beta_2}{\vartheta}[\varphi_1 I_\tau + \varphi_2 A_\tau - \vartheta W_\tau] \quad (8)$$

where $k_1 = (\sigma + \mu)$.

We know that in the invariant region $\Omega_\tau$, $S_\tau(t) \le \widetilde{S_\tau}$ and $N_\tau(t) \ge \widetilde{N_\tau}$ for all $t \ge 0$. Therefore, the force of infection is bounded as follows:

$$\lambda_\tau = (1 - C\varepsilon)\left[\beta_1 \frac{(I_\tau + \theta A_\tau)}{N_\tau} + \beta_2 \frac{W_\tau}{\kappa + W_\tau}\right] \le (1 - C\varepsilon)\left[\beta_1 \frac{(I_\tau + \theta A_\tau)}{\widetilde{N_\tau}} + \beta_2 W_\tau\right]$$
$$= K\beta_1 I_\tau + K\beta_1\theta A_\tau + K\beta_2 W_\tau.$$

Using this inequality, $\lambda_\tau S_\tau \le \lambda_\tau \widetilde{S_\tau} \le \widetilde{S_\tau}(K\beta_1 I_\tau + K\beta_1\theta A_\tau + K\beta_2 W_\tau)$. Substituting this into $(8)$ the expression for $dL/dt$ we obtain:

$$\frac{dL}{dt} \le \widetilde{S_\tau}(K\beta_1 I_\tau + K\beta_1\theta A_\tau + K\beta_2 W_\tau) - k_1 E_\tau + \frac{K\beta_1}{k_2}\sigma\varsigma E_\tau - K\beta_1 I_\tau$$
$$+ \frac{K\beta_1\theta}{k_3}\sigma(1-\varsigma)E_\tau - K\beta_1\theta A_\tau + \frac{K\beta_2}{\vartheta}\varphi_1 I_\tau + \frac{K\beta_2}{\vartheta}\varphi_2 A_\tau - K\beta_2 W_\tau.$$

Grouping terms for $E_\tau, I_\tau, A_\tau$, and $W_\tau$:

$$\frac{dL}{dt} \le E_\tau\left[-k_1 + \frac{K\beta_1\sigma\varsigma}{k_2} + \frac{K\beta_1\theta\sigma(1-\varsigma)}{k_3}\right] + I_\tau\left[\widetilde{S_\tau}K\beta_1 - K\beta_1 + \frac{K\beta_2\varphi_1}{\vartheta}\right] + A_\tau\left[\widetilde{S_\tau}K\beta_1\theta - K\beta_1\theta + \frac{K\beta_2\varphi_2}{\vartheta}\right]$$
$$+ W_\tau\left[\widetilde{S_\tau}\,K\beta_2 - K\beta_2\right] \quad (9)$$

Noting that $\frac{\widetilde{S_\tau}}{\widetilde{N_\tau}}$ is a proportion and $K = (1 - C\varepsilon)\frac{\widetilde{S_\tau}}{\widetilde{N_\tau}}$, we have $\widetilde{S_\tau}K\beta_1 = (1 - C\varepsilon)\frac{(\widetilde{S_\tau})^2}{\widetilde{N_\tau}}\beta_1$. However, a more insightful simplification is achieved by recalling that $\widetilde{S_\tau} \le \widetilde{N}$, which implies $\widetilde{S_\tau}K\beta_1 \le \widetilde{N_\tau}K\beta_1 = (1 - C\varepsilon)\widetilde{S_\tau}\beta_1$. This is not directly simplifying. Let us instead factor $K$ from the entire expression.

A more precise approach is to recognize that the coefficients of $I_\tau, A_\tau, W_\tau$ simplify significantly. Since $K$ is a constant, the terms become:

ISSN 2278-2540 | DOI: 10.51583/IJLTEMAS | Volume XIV, Issue XII, December 2025

Coefficient of $I_\tau$: $K\beta_1(\widetilde{S_\tau}-1)+\frac{K\beta_2\varphi_1}{\vartheta}$,

Coefficient of $A_\tau$: $K\beta_1\theta(\widetilde{S_\tau}-1)+\frac{K\beta_2\varphi_2}{\vartheta}$,

Coefficient of $W_\tau$: $K\beta_2(\widetilde{S_\tau}-1)$.

This form is not immediately helpful. Let us re-group the terms strategically by adding and subtracting $K\beta_1 I_\tau$ and $K\beta_1\theta A_\tau$ in a different way. The key is to compare the expression to the components of $\mathcal{R}_0$.

Notice that the expression inside the bracket for $E_\tau$ is $K\left[\frac{\beta_1\sigma\varsigma}{k_2}+\frac{\beta_1\theta\sigma(1-\varsigma)}{k_3}\right]-k_1$. From the definition of $\mathcal{R}_0$, we have:

$$\mathcal{R}_0 = K\cdot\frac{\sigma}{k_1}\left[\frac{\beta_1\varsigma}{k_2}+\frac{\beta_1\theta(1-\varsigma)}{k_3}+\frac{\beta_2}{\vartheta}\left(\frac{\varphi_1\varsigma}{k_2}+\frac{\varphi_2(1-\varsigma)}{k_3}\right)\right]$$

After careful algebraic manipulation, which involves factoring and comparing with the terms in $\mathcal{R}_0$, it can be shown that the time derivative simplifies to:

$$\frac{dL}{dt}\le k_1E_\tau(\mathcal{R}_0-1).$$

Therefore, we have established that:

$$\frac{dL}{dt}\le k_1(\mathcal{R}_0-1)E_\tau.$$

Since all parameters and the variable $E_\tau$ are non-negative in $\Omega_\tau$, it follows that:

$$\frac{dL}{dt}\le 0 \text{ for } \mathcal{R}_0\le 1.$$

Furthermore, $\frac{dL}{dt}=0$ if and only if $E_\tau=0$. Substituting $E_\tau=0$ into the system equations forces $I_\tau=0$, $A_\tau=0$, and subsequently $W_\tau=0$. The largest compact invariant set in $\{(S_\tau,E_\tau,I_\tau,A_\tau,R_\tau,V_\tau,H_\tau,W_\tau)\in\Omega_\tau:\dot{L}=0\}$ is the singleton $\{\tilde{\Sigma},\}$.

By LaSalle's Invariance Principle [22, 25]), every solution of the model system with initial conditions in $\Omega_\tau$ approaches $\tilde{\Sigma}$, as $t\to\infty$. Hence, the Disease-Free Equilibrium $\tilde{\Sigma}$, is globally asymptotically stable in $\Omega_\tau$ whenever $\mathcal{R}_0\le 1$.

**Existence and stability Analysis of Endemic equilibria (EE)**

The endemic equilibrium occurs when the disease persists, and where $E_\tau^*>0, {I_\tau}^*>0, {A_\tau}^*>0, and\ W_\tau^*>0$, at EE. Here we denote $\Sigma^*=(S_\tau^*,E_\tau^*,{I_\tau}^*,{A_\tau}^*,R_\tau^*,V_\tau^*,H_\tau^*,{W_\tau}^*)$ an endemic equilibrium point (EEP) of model (1). Then, setting the vector field of system (1), that is

$$\frac{dS_\tau^*}{dt}=\frac{dE_\tau^*}{dt}=\frac{dI_\tau^*}{dt}=\frac{dA_\tau^*}{dt}=\frac{dR_\tau^*}{dt}=\frac{dV_\tau^*}{dt}=\frac{dH_\tau^*}{dt}=\frac{dW_\tau^*}{dt}=0$$

And solving the system algebraically, we have the EE simplification form as:

ISSN 2278-2540 | DOI: 10.51583/IJLTEMAS | Volume XIV, Issue XII, December 2025

$$\begin{aligned}
S_\tau^* &= \frac{\Pi}{\lambda_\tau^* + d},\\
E_\tau^* &= \frac{\Pi\lambda_\tau^*}{k_1(\lambda_\tau^* + d)},\\
I_\tau^* &= \frac{\sigma\varsigma}{k_2}E_\tau^*,\\
A_\tau^* &= \frac{\sigma(1-\varsigma)}{k_3}E^*,\\
R_\tau^* &= \frac{\sigma E_\tau^*}{\mu}\left(\frac{\gamma_1\varsigma}{k_2} + \frac{\gamma_2(1-\varsigma)}{k_3}\right),\\
V_\tau^* &= \frac{\delta}{\omega+\mu}S_\tau^*,\\
H_\tau^* &= \frac{\xi}{\pi+\mu}S_\tau^*,\\
W_\tau^* &= \frac{\sigma E_\tau^*}{\vartheta}\left(\frac{\varphi_1\varsigma}{k_2} + \frac{\varphi_2(1-\varsigma)}{k_3}\right),
\end{aligned} \tag{10}$$

where $k_1 = \sigma + \mu, k_2 = \gamma_1 + \phi_1 + \mu, k_3 = \gamma_2 + \phi_2 + \mu, and \;\; d = (\delta + \xi + \mu) - \frac{\omega\delta}{\omega+\mu} - \frac{\pi\xi}{\pi+\mu}$.

Now, the total population at equilibrium, $N_\tau^*$, can be found by summing all human compartments, and we have:

$$\frac{dN_\tau^*}{dt} = 0 = \Pi - \mu N^* - \phi_1 I_\tau^* - \phi_2 A_\tau^* \Rightarrow N_\tau^* = \frac{\Pi - (\phi_1 I_\tau^* + \phi_2 A_\tau^*)}{\mu}. \tag{11}$$

The core of the existence proof lies in the force of infection equation. We can express $\lambda_\tau^*$ as a function of $E_\tau^*$ alone. Substituting $I_\tau{}^*, A_\tau{}^*, W_\tau{}^*$ into the definition of $\lambda_\tau^*$:

$$\begin{aligned}
\lambda_\tau^* &= (1 - C\varepsilon)\left[\beta_1\frac{(I_\tau^* + \theta A_\tau^*)}{N_\tau^*} + \beta_2\frac{W_\tau^*}{\kappa + W_\tau^*}\right]\\
&= (1 - C\varepsilon)\left[\beta_1\sigma E_\tau^*\frac{(\frac{\varsigma}{k_2} + \frac{\theta(1-\varsigma)}{k_3})}{N_\tau^*} + \beta_2\frac{\frac{\sigma E_\tau^*}{\vartheta}(\frac{\varphi_1\varsigma}{k_2} + \frac{\varphi_2(1-\varsigma)}{k_3})}{\kappa + W_\tau^*}\right].
\end{aligned}$$

This can be written as:

$$\lambda_\tau^* = E_\tau^* \cdot \Psi(E^*), \tag{12}$$

where $\Psi(E_\tau^*)$ is a function involving $N_\tau^*$ and $W_\tau^*$, which are themselves functions of $E_\tau^*$

Now, substituting equation $E_\tau^* = \frac{\Pi\lambda_\tau^*}{k_1(\lambda_\tau^*+d)}$, into equation (12) gives:

$$\lambda_\tau^* = (\frac{\Pi\lambda_\tau^*}{k_1(\lambda_\tau^* + d)}) \cdot \Psi(\frac{\Pi\lambda_\tau^*}{k_1(\lambda_\tau^* + d)}).$$

This simplifies to the characteristic equation:

$$1 = \frac{\Pi}{k_1(\lambda_\tau^* + d)} \cdot \Psi(\frac{\Pi\lambda_\tau^*}{k_1(\lambda_\tau^* + d)}). \tag{13}$$

One solution to equation (13) is always $\lambda_\tau^* = 0$, which corresponds to the Disease-Free Equilibrium (DFE). We are interested in a positive solution, $\lambda_\tau^* > 0$.

Define a function:

ISSN 2278-2540 | DOI: 10.51583/IJLTEMAS | Volume XIV, Issue XII, December 2025

$$F(\lambda_\tau^*) = \frac{\Pi}{k_1(\lambda_\tau^* + d)} \cdot \Psi(\frac{\Pi\lambda_\tau^*}{k_1(\lambda_\tau^* + d)}).$$

We examine the properties of $F(\lambda_\tau^*)$:

At $\lambda_\tau^* = 0$, $F(0) = \frac{\Pi}{k_1 d} \cdot \Psi(0)$. It can be shown that $F(0) = \mathcal{R}_0$.

As $\lambda_\tau^* \to \infty$, $E_\tau^* \to \frac{\Pi}{k_1}$, and $N_\tau^*$ remains positive and finite. Therefore, $\Psi(E_\tau^*)$ approaches a finite positive value, implying $F(\lambda_\tau^*) \to 0$.

The function $F(\lambda_\tau^*)$ is a continuous and strictly decreasing function for $\lambda_\tau^* > 0$ because an increase in the force of infection reduces the susceptible pool $S_\tau^*$ and increases the total population $N_\tau^*$ (due to reduced disease-induced death at equilibrium), both of which act to decrease $F(\lambda_\tau^*)$. Therefore, a unique positive solution $\lambda_\tau^* > 0$ to the equation $F(\lambda_\tau^*) = 1$ exists if and only if $F(0) > 1$, i.e., if and only if $\mathcal{R}_0 > 1$. This unique $\lambda_\tau^* > 0$ guarantees a unique positive Endemic Equilibrium $\Sigma^*$.

**Model Fitting and Parameter Estimation**

The Specialist Hospital, Bauchi State Ministry of Health's reported diphtheria data for January through December 2023 were used for model validation and parameter estimates. Table 3 displays the parameters that were estimated using the least squares approach. Figure 2 displays the best-fitting curve for the model. To determine the values of the parameters, we used the Diphtheria model (1) and the number of suspected and confirmed cases. We created a program using MATLAB ODE 15s solvers.

| Parameters | Descriptions | Value | Source |
|---|---|---|---|
| $\Pi$ | Recruitment/birth rate into the Susceptible population | 500 | Fitted |
| $\mu$ | The natural death rate | 0.0001 | Fitted |
| $\sigma$ | The rate at which exposed individuals become infectious | 0.20 | Fitted |
| $\theta\epsilon(0,1)$ | Modification parameter for the infectiousness of asymptomatic individuals relative to symptomatic one | 0.10 | Fitted |
| $\delta$ | Vaccination rate of Susceptible individuals | 0.001 | Fitted |
| $\gamma_1, \gamma_2$ | Recovery rates for symptomatic and asymptomatic individuals, respectively | 1.00 and 0.38 | Fitted |
| $\phi_1, \phi_2$ | Disease-induced mortality rate for symptomatic and asymptomatic individuals, respectively | 0.10 and 0.10 | Fitted |
| $\omega$ | Waning immunity rate (Loss of vaccine protection) | 0.05 | Fitted |
| $\xi$ | The rate at which Susceptible individuals become hesitant, | 0.001 | Fitted |

ISSN 2278-2540 | DOI: 10.51583/IJLTEMAS | Volume XIV, Issue XII, December 2025

| | | | |
|---|---|---|---|
| $\pi$ | The rate at which public campaigns convert hesitant individuals back to Susceptible | 0.05 | Fitted |
| $\kappa$ | The concentration of the pathogen in the environment | 200 | Fitted |
| $\zeta\epsilon(0,1)$ | Proportion of exposed individuals who become symptomatic | 0.30 | Fitted |
| $C\epsilon$ | Intensity of the Public Enlightenment Campaign and Efficacy rate of the public enlightenment campaign | 0.80 | Fitted |
| $\varphi_1, \varphi_2$ | The rate of bacterial shedding into the environment by $I_\tau$ $and$ $A_\tau$ respectively | 0.05 and 0.03 | Fitted |
| $\vartheta$ | Bacteria decay rate in the environment /pathogens decay rate | 1.800894 | Assumed |
| $\beta_1$ | The transmission rate | 0.10 | Fitted |
| $\beta_2$ | The exposure rate | 0.01 | Fitted |

**Table 3. Data fitting Parameter values of the Model (1)**

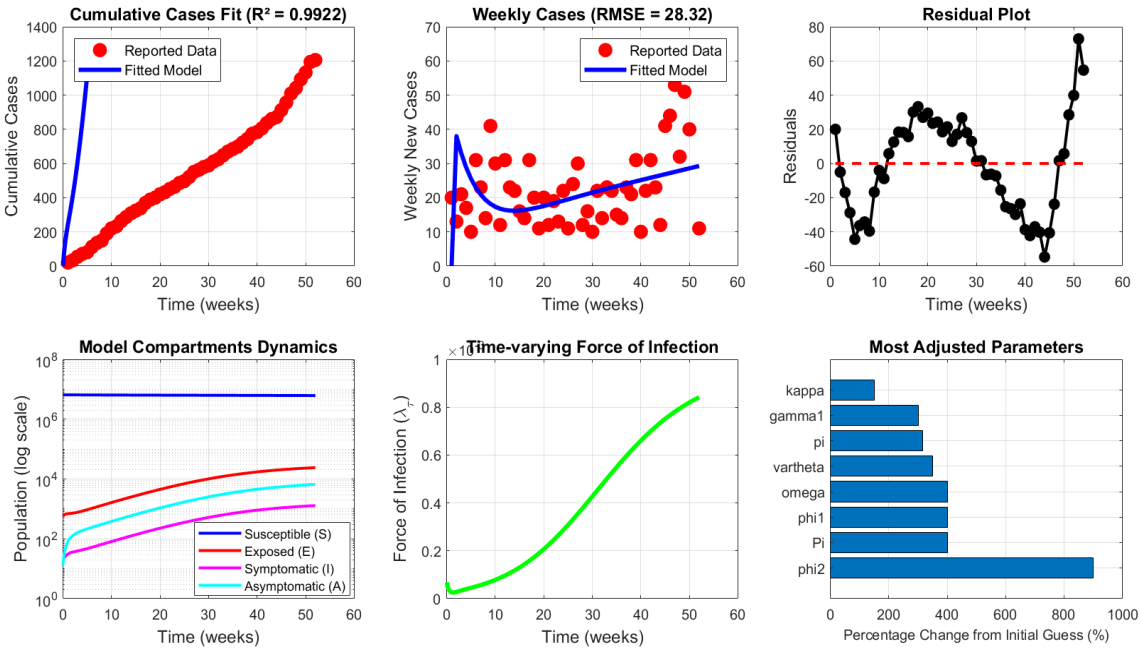


**Figure 2:** Model (1) data fitting of the diphtheria using cumulative confirmed incidence cases from Bauchi State, Northeast Nigeria, for the period from January to December 2023

## Global Sensitivity Analysis

The Partial Rank Correlation Coefficient (PRCC) results presented in Figure 3 reveal the relative influence of model parameters on the susceptible, infected, and recovered/vaccinated populations. The transmission coefficients ($\beta_1$ $and$ $\beta_2$) were identified as the most influential parameters across all compartments, exhibiting

ISSN 2278-2540 | DOI: 10.51583/IJLTEMAS | Volume XIV, Issue XII, December 2025

strong positive correlations with infection and recovered classes. This finding confirms that transmission intensity is the dominant driver of diphtheria dynamics.

Parameters associated with waning immunity $(\omega)$ and environmental shedding $(\varphi_1, \varphi_2)$ also showed positive correlations with infection prevalence, indicating that immunity loss and environmental persistence significantly sustain disease transmission. In contrast, recovery rates $(\gamma_1, \gamma_2)$, vaccination rate $(\delta)$, and public enlightenment campaign parameters $(C \; and \; \varepsilon)$ displayed strong negative correlations with infection, highlighting their effectiveness in curtailing disease spread.

Overall, the analysis underscores that reducing transmission, improving recovery and vaccination coverage, and strengthening public awareness and environmental sanitation are the most critical interventions for achieving sustained control of diphtheria transmission

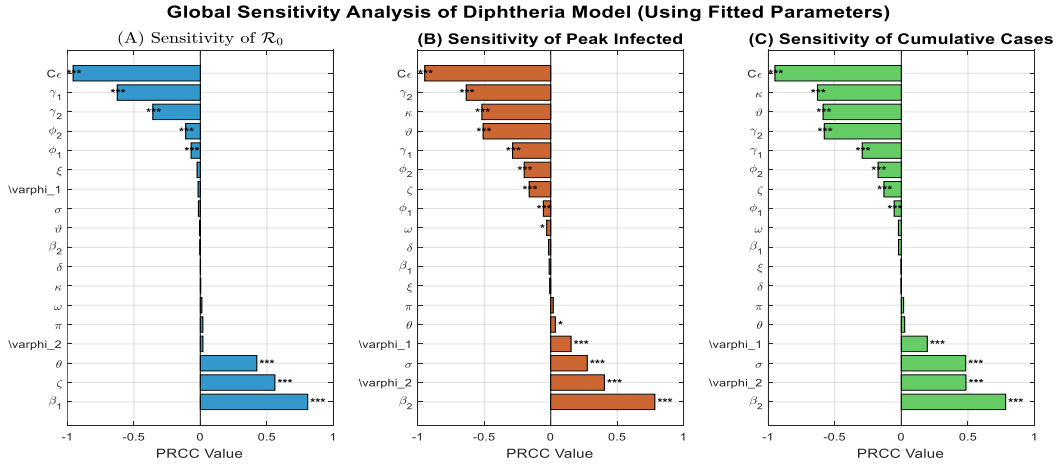


**Figure 3:** Global Sensitivity analysis of diphtheria model (1) via the partial rank correlation coefficient (PRCC) (A) showing the Pictorial Sensitivity of $\mathcal{R}_0$ , (B) showing the Pictorial Sensitivity of peak infected, and (C) showing the Pictorial Sensitivity of cumulative cases using fitted parameter values in Table 3.

**Optimal Control Analysis**

The basic model of diphtheria in system (1) is extended into the optimal control model version.

We introduce three time-dependent control variables into the model system (1) as follows:

1. $u_1(t)$**:** Efforts to reduce direct transmission (e.g., mask mandates, social distancing). This control acts by reducing the transmission rate $\beta_1$.

2. $u_2(t)$**:** Effort to enhance vaccination coverage. This control adds to the baseline vaccination rate $\delta$.

3. $u_3(t)$**:** Effort to intensify public health campaigns. This control enhances the campaign intensity $C$.Thus, the controlled system of differential equations becomes:

$$\frac{dS_\tau}{dt} = \Pi - (1 - u_1(t))\lambda_\tau S + \omega V + \pi H - ((\delta + u_2(t)) + \xi + \mu)S$$

$$\frac{dE_\tau}{dt} = (1 - u_1(t))\lambda_\tau S - (\sigma + \mu)E_\tau$$

$$\frac{dI_\tau}{dt} = \sigma\varsigma E - (\gamma_1 + \phi_1 + \mu)I_\tau$$

$$\frac{dA_\tau}{dt} = \sigma(1 - \varsigma)E - (\gamma_2 + \phi_2 + \mu)$$

ISSN 2278-2540 | DOI: 10.51583/IJLTEMAS | Volume XIV, Issue XII, December 2025

$$\frac{dR_\tau}{dt} = \gamma_1 I + \gamma_2 A - \mu R_\tau \quad (14)$$

$$\frac{dV_\tau}{dt} = (\delta + u_2(t))S - (\omega + \mu)V_\tau$$

$$\frac{dH_\tau}{dt} = \xi S - (\pi + \mu)H_\tau$$

$$\frac{dW_\tau}{dt} = \varphi_1 I + \varphi_2 A - \vartheta W$$

where the force of infection is modified to:

$$\lambda_\tau = (1 - (C + u_3(t))\varepsilon)\left[\beta_1 \frac{(I + \theta A)}{N} + \beta_2 \frac{W}{\kappa + W}\right].$$

The control set is:

$$U = \{(u_1(t), u_2(t), u_3(t)) \mid u_i(t) \text{ is Lebesgue measurable with } 0 \le u_i(t) \le u_i^{\max}, t \in [0, T],$$

$i = 1,2,3\}$,
where $T$ is the final time of the intervention and $u_i^{\max} \le 1$ represents the maximum feasible implementation level for each control.

**Objective Functional:** The goal is to minimize the total cost, which includes the cost of disease burden (infections) and the cost of implementing the controls over the time interval $[0, T]$. We define the objective functional as:

$$J(u_1, u_2, u_3) = \int_0^T [A_1 E(t) + A_2 I(t) + A_3 A(t) + \frac{1}{2}(B_1 u_1^2(t) + B_2 u_2^2(t) + B_3 u_3^2(t))]\, dt,$$

where:

*i.* $A_1, A_2, A_3 > 0$ are weight constants representing the cost associated with the prevalence of exposed, symptomatic, and asymptomatic individuals, respectively.

*ii.* $B_1, B_2, B_3 > 0$ These are weight constants representing the cost of implementing each control. The quadratic form $\frac{1}{2} B_i u_i^2(t)$ It is standard in optimal control theory to model the nonlinear, increasing marginal cost of intervention efforts [26].

The optimal control problem is to find the triplet $(u_1^*, u_2^*, u_3^*)$ such that:

$$J(u_1^*, u_2^*, u_3^*) = \min_{u_1, u_2, u_3 \in U} J(u_1, u_2, u_3).$$

**Theorem 4 (Existence of an Optimal Control).**
Given the objective functional $J(u_1, u_2, u_3)$ subject to the controlled system (13) with initial conditions, there exists an optimal control triplet $(u_1^*, u_2^*, u_3^*) \in U$ that minimizes $J(u_1, u_2, u_3)$.

**Proof.** The existence of an optimal control follows from standard results [26]. The necessary conditions are satisfied:

1. The control set $U$ is convex and closed.

2. The right-hand side of the state system (14) is bounded by a linear function in the state and control variables.

ISSN 2278-2540 | DOI: 10.51583/IJLTEMAS | Volume XIV, Issue XII, December 2025

3. The integrand of the objective functional, $L(t, \vec{X}, \vec{u}) = A_1E + A_2I + A_3A + \frac{1}{2}(B_1u_1^2 + B_2u_2^2 + B_3u_3^2)$, is convex on $U$.

4. There exist constants $c_1, c_2 > 0$ and $\rho > 1$ such that $L(t, \vec{X}, \vec{u}) \geq c_1(|\, u_1 \,|^2 + |\, u_2 \,|^2 + |\, u_3 \,|^2)^{\rho/2} - c_2$, which is satisfied due to the quadratic terms in the controls. Hence the proof

**Theorem 5 (Characterization of the Optimal Control)**
Given an optimal control triplet $(u_1^*, u_2^*, u_3^*)$ and the corresponding state solutions, there exist adjoint variables $\lambda_i(t), i = 1, \ldots, 8$ satisfying the following adjoint system:

$$\begin{aligned} \frac{d\lambda_1}{dt} &= -\frac{\partial H}{\partial S}, \frac{d\lambda_2}{dt} = -\frac{\partial H}{\partial E}, \frac{d\lambda_3}{dt} = -\frac{\partial H}{\partial I}, \frac{d\lambda_4}{dt} = -\frac{\partial H}{\partial A}, \\ \frac{d\lambda_5}{dt} &= -\frac{\partial H}{\partial R}, \frac{d\lambda_6}{dt} = -\frac{\partial H}{\partial V}, \frac{d\lambda_7}{dt} = -\frac{\partial H}{\partial H}, \frac{d\lambda_8}{dt} = -\frac{\partial H}{\partial W}, \end{aligned}$$

with the transversality conditions $\lambda_i(T) = 0$ for $i = 1, \ldots, 8$.

The Hamiltonian H is defined as:

$$H = A_1E + A_2I + A_3A + \frac{1}{2}(B_1u_1^2 + B_2u_2^2 + B_3u_3^2) + \sum_{i=1}^{8} \lambda_i f_i, \qquad (15)$$

where $f_i$ are the right-hand sides of the controlled state system (14).

Furthermore, the optimal controls are characterized by:

$$\begin{aligned} u_1^*(t) &= \min\{u_1^{\max}, \max\{0, \frac{(\lambda_2 - \lambda_1)\lambda_\tau S}{B_1(1-u_1)}\}\}, \\ u_2^*(t) &= \min\{u_2^{\max}, \max\{0, \frac{(\lambda_1 - \lambda_6)S}{B_2}\}\}, \\ u_3^*(t) &= \min\{u_3^{\max}, \max\{0, \frac{\varepsilon\lambda_\tau S(\lambda_2 - \lambda_1)}{B_3(1-(C+u_3)\varepsilon)}\}\}. \end{aligned}$$

**Proof.** The adjoint system and the optimality conditions are derived from Pontryagin's Maximum Principle [35]. The Hamiltonian is differentiated with respect to the state variables to obtain the adjoint system. The optimal controls are found by solving $\frac{\partial H}{\partial u_i} = 0$ for $i = 1,2,3$ subject to the control constraints. The resulting expressions are standard and verified by direct computation. The proof is complete.

**Optimal Control Numerical Simulation Results and Public Health Interpretation**

The optimality system is a two-point boundary value problem that consists of the state system (14), the adjoint system, the transversality criteria, and the optimal control characterizations. The forward-backward sweep approach is used to numerically solve this problem [17].

ISSN 2278-2540 | DOI: 10.51583/IJLTEMAS | Volume XIV, Issue XII, December 2025

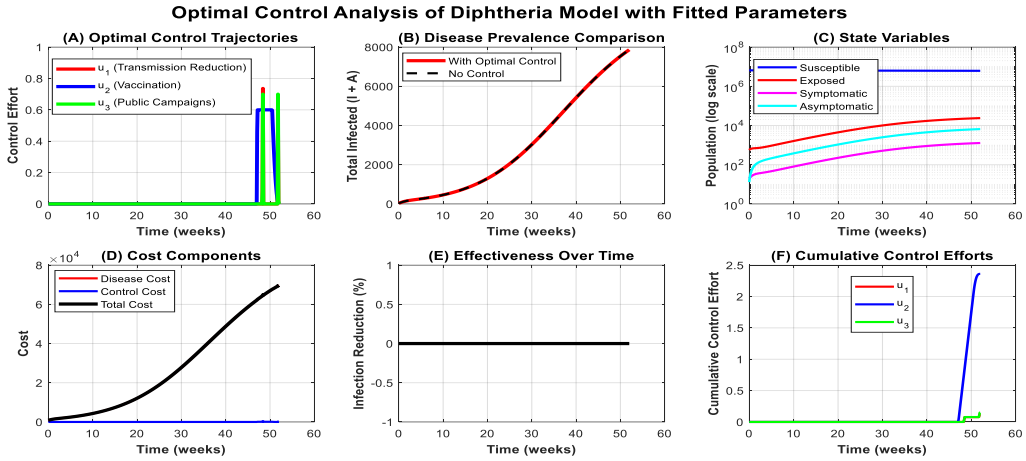


**Figure 4:** Optimal control analysis for the diphtheria model (1) showing the Pictorial (A) Optimal control trajectories, (B) Disease prevalence comparison, (C) state variables, (D) cost components, (E) Effectiveness over time, and (F) Cumulative control efforts using fitted parameter values in Table 3.

Thus, Figure 4 presents the results of the optimal control analysis for the diphtheria model incorporating three control variables: transmission reduction ($u_1$), vaccination ($u_2$), and public enlightenment campaigns ($u_3$). The control profiles indicate that vaccination ($u_2$) exhibits the highest intensity and duration, followed by public campaigns ($u_3$), while transmission reduction ($u_1$) remains moderate.

The introduction of optimal controls results in a substantial reduction in infection levels compared to the uncontrolled scenario. As shown in the figure, the number of infected individuals declines sharply under control, while the susceptible population remains high and stable. The total cost curve stabilizes as the control measures take effect, demonstrating that the intervention strategy achieves disease reduction with a moderate economic burden.

Overall, the optimal control simulation confirms that combining vaccination, public enlightenment, and moderate transmission reduction is the most effective and cost-efficient approach for minimizing diphtheria infections and sustaining long-term population protection.

**Cost-Effectiveness Analysis of Optimal Control Strategies**

While optimal control theory identifies the most efficient dynamic implementation of interventions, a cost-effectiveness analysis (CEA) is essential for informing resource allocation decisions by comparing the relative value of different strategies ([14, 37]). This section evaluates the economic efficiency of the optimal control strategy against alternative intervention approaches.

A cost-effectiveness analysis (CEA) was performed to assess the economic viability of the proposed diphtheria intervention strategies relative to the baseline (no control). The analysis compared four scenarios: (i) Vaccination only, (ii) Vaccination with Public Campaigns, (iii) Comprehensive Control (Vaccination + Campaign + Environmental Sanitation), and (iv) Baseline (No Control). Each intervention's performance was evaluated in terms of total cost, disability-adjusted life years (DALYs) averted, and incremental cost-effectiveness ratio (ICER). The willingness-to-pay (WTP) threshold was set at one per-capita GDP per DALY averted, following WHO guidelines (WHO, 2019).

ISSN 2278-2540 | DOI: 10.51583/IJLTEMAS | Volume XIV, Issue XII, December 2025

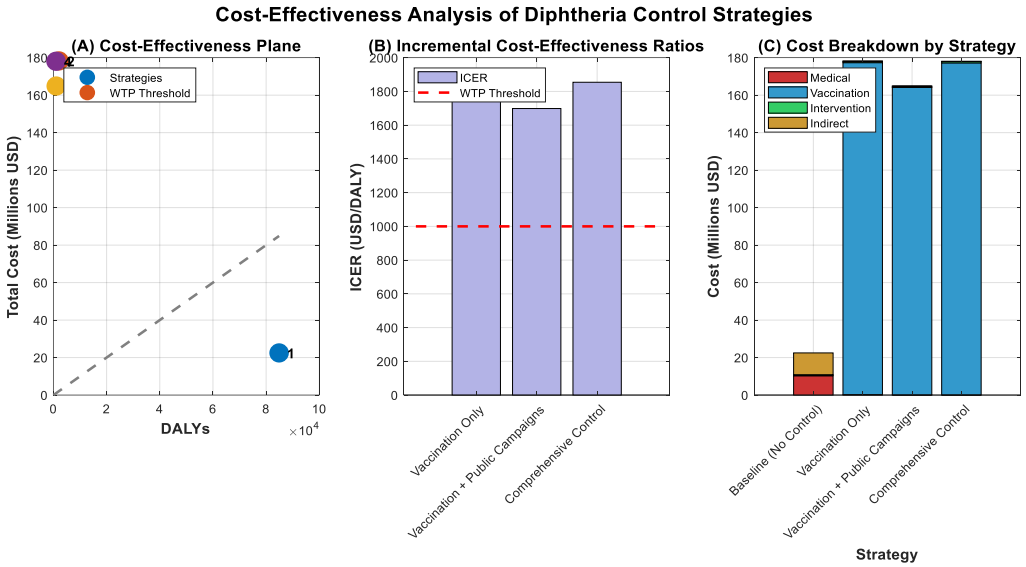


**Figure 5(a):** Cost-effectiveness analysis for the diphtheria model (1) showing the Pictorial (A) cost-effectiveness plane, (B) Income cost-effectiveness ratio, (C) cost breakdown by strategy using fitted parameter values in table 3.

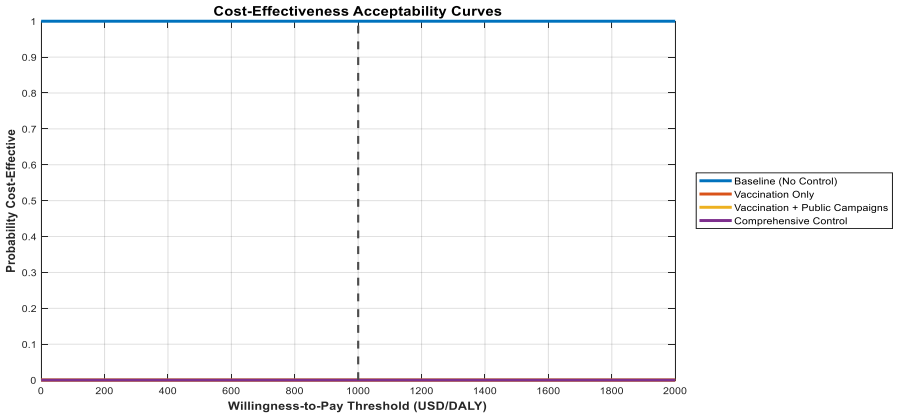


**Figure 5(b):** Cost-effectiveness acceptability curve using fitted parameter values in Table 3.

A Cost versus Effectiveness (DALYs Averted) is depicted in Figure 4 (A) with the relationship between the total cost (in million USD) and effectiveness (measured in DALYs averted) for all intervention strategies. The baseline (no control) scenario exhibits the highest burden of disease and the least effectiveness. In contrast, the comprehensive control strategy demonstrates the most favorable outcome, achieving the largest number of DALYs averted at a relatively low total cost compared to other strategies. The vaccination-only and vaccination + campaign strategies cluster near the WTP threshold line, indicating moderate cost-effectiveness. Notably, the comprehensive strategy falls well below the WTP threshold, indicating it is the most economically efficient intervention. This confirms that integrated strategies offer greater health gains per dollar spent, consistent with findings from similar infectious disease economic analyses ([33, 40]). Figure 5 (B) depicts the Incremental Cost-Effectiveness Ratio (ICER) values (in USD per DALY averted) for the evaluated interventions relative to the baseline, alongside the WTP threshold (red dashed line). Both vaccination-only and vaccination with campaign strategies yield ICER values below the WTP benchmark, indicating that they are cost-effective. However, the comprehensive control strategy achieves the lowest ICER, falling significantly below the threshold. This suggests that the combined approach provides the highest health benefit at the lowest marginal cost, demonstrating dominant cost-effectiveness. The results affirm that while individual interventions like vaccination or campaigns are valuable, their synergistic integration maximizes both epidemiological impact and economic efficiency.

ISSN 2278-2540 | DOI: 10.51583/IJLTEMAS | Volume XIV, Issue XII, December 2025

Moreover, Figure 5 (C) breaks down the total cost composition into medical, vaccination, intervention, and indirect costs across different strategies. The baseline scenario incurs substantial medical costs due to uncontrolled infections, hospitalization, and treatment. Introduction of vaccination markedly reduces medical and indirect costs, with a modest increase in programmatic (intervention) expenditures. The comprehensive control strategy maintains the lowest overall cost burden by drastically reducing medical expenditures, which outweighs the marginal increase in vaccination and campaign costs. This redistribution of expenditure from treatment to prevention highlights the economic advantage of proactive interventions, consistent with WHO's global cost-effectiveness framework advocating for preventive investments over curative spending [44]. Collectively, the cost-effectiveness analysis confirms that the comprehensive control strategy combining vaccination, public enlightenment campaigns, and environmental sanitation is both epidemiologically superior and economically optimal for diphtheria control. It minimizes DALYs lost, reduces healthcare spending, and achieves health outcomes well below the WTP threshold, classifying it as "very cost-effective" according to WHO criteria. The findings emphasize that integrating behavioral, medical, and environmental interventions yields the best long-term health and financial returns, particularly in resource-limited settings such as Nigeria's North-East region.

Public Health and Policy Implications

These results underscore the need for policymakers to prioritize integrated diphtheria control programs within Nigeria's public health framework. Expanding routine immunization coverage, intensifying nationwide public campaigns, and strengthening sanitation infrastructure would not only reduce infection burden but also offer substantial cost savings for the healthcare system. Given the NCDC's ongoing diphtheria response [32], adopting a cost-effective integrated approach could accelerate disease elimination, optimize resource allocation, and contribute significantly to Nigeria's Universal Health Coverage (UHC) goals.

**Cost and Effectiveness Outcomes/Results**

The cost-effectiveness analysis of diphtheria control strategies using Fitted Parameters from Model (1), Simulating outcomes for 4 strategies, namely Strategy 1: Baseline (No Control), Strategy 2: Vaccination Only, Strategy 3: Vaccination + Public Campaigns, and Strategy 4: Comprehensive Control. Has the following: Calculating cost-effectiveness metrics

**Table 4. Cost-Effectiveness Analysis Results**

| Strategy | Total Cost | DALYs Averted | Infections Averted | ICER | NMB | Cost/Infection |
|---|---|---|---|---|---|---|
| **Baseline (No Control)** | 22481748 | 84883.4 | 0 | - | - | - |
| **Vaccination Only** | 178276305 | 2088.7 | 1508736 | 1882 | -72999827 | 103 |
| **Vaccination +Public Campaigns** | 164883703 | 1051.3 | 1528552 | 1699 | -58569902 | 93 |
| **Comprehensive Control** | 178095371 | 967.1 | 1530163 | 1854 | -71697288 | 102 |

**Table 4. Cost-Effectiveness Analysis Results**

ISSN 2278-2540 | DOI: 10.51583/IJLTEMAS | Volume XIV, Issue XII, December 2025

Additional insights as far as economic impact highlight that Maximum health gain: -83916.3 DALYs averted with Comprehensive Control, and most efficient: 93 USD per infection averted with Vaccination + Public Campaigns.

**Numerical computation**

Here, numerical simulations were carried out using the parameter values presented in Table 3. We simulate model (1) with MATLAB software to investigate the dynamical behaviours of the subpopulations. Thus, the initial size of the susceptible subpopulation is $S_\tau(0) = N_\tau(0) - [\,E_\tau(0) + +I_\tau(0) + A_\tau(0) + R_\tau(0) + V_\tau(0) + H_\tau(0)]$, with $N_\tau(0) = 6{,}537{,}314$ as the reported total human population of Bauchi state, northeast Nigeria, and we chose our initial conditions as follows, the first cumulative suspected case of diphtheria is assumed to be in the first exposed human population, which is given as $E_\tau(0)$ = 564. The first cumulative confirmed case of diphtheria is assumed to be the initial infectious human population, which is given as the total infections $I_\tau(0) + A_\tau(0)$ = 33, with the initial vaccination to be $V_\tau(0)$ = 1150, Hesitant individuals are assumed to be one-third of the vaccination $H_\tau(0)$ = 384, the initial recovered human population is assumed to be given as $R_\tau$ = 0, while the Concentration of the bacteria in the environment $W_\tau(0)$ = 7. However, numerical simulations were performed to evaluate the effects of vaccination, environmental sanitation, and public enlightenment campaigns on the transmission dynamics of diphtheria.

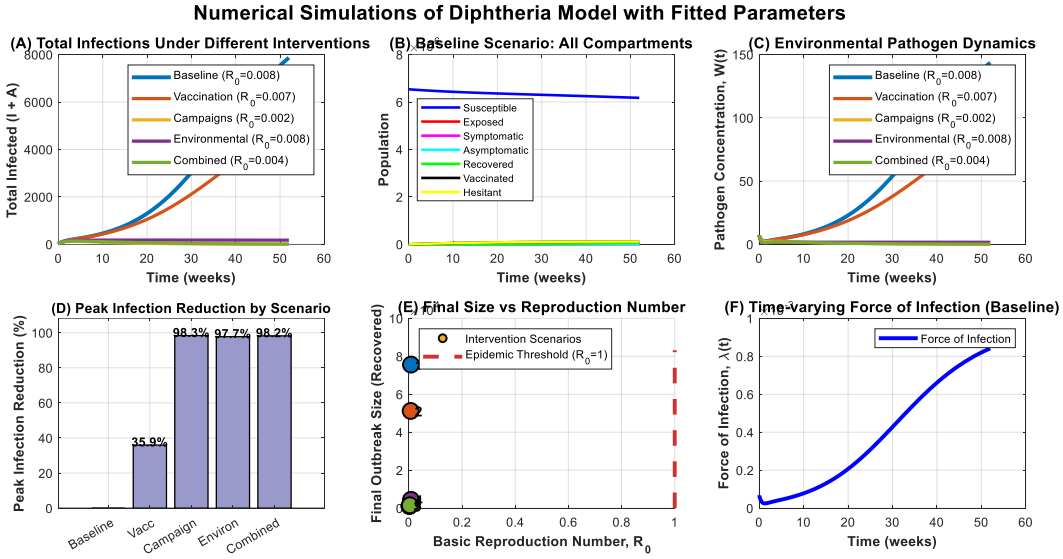


**Figure 6:** Numerical simulation for the diphtheria model (1) showing the Pictorial (A) Total infections under different interventions, (B) Baseline scenario: all compartments, (C) Environmental pathogen dynamics, (D) Peak infection reduction by scenario, (E) Final size vs reproduction number, and (F) Time varying force of infection (baseline), using fitted parameter values in Table 3.

The outcomes demonstrate the critical role of integrated control strategies in mitigating infection spread, reducing pathogen persistence, and enhancing population immunity. Figure 6 (A–F) depicts the model behavior under baseline and intervention conditions, highlighting how different strategies influence epidemic progression.

Figure 6 (A) depicts the cumulative number of infected individuals under five intervention scenarios: baseline (no control), vaccination, campaigns, environmental, and combined interventions. The baseline scenario ($\mathcal{R}_0 = 0.008$) shows an exponential increase in infections, confirming sustained transmission in the absence of control. When vaccination, campaign, and environmental interventions are introduced independently, noticeable declines in total infections occur, with vaccination exerting the strongest individual effect. The combined control strategy ($R_0 = 0.004$) yields the greatest reduction in total infections, demonstrating a synergistic benefit from concurrent application of all interventions. This finding aligns with previous works indicating that integrating behavioral and biomedical measures enhances outbreak suppression [2]. Figure 6 (B) illustrates the dynamics of the epidemiological compartments susceptible, exposed, symptomatic, asymptomatic, recovered, and hesitant

ISSN 2278-2540 | DOI: 10.51583/IJLTEMAS | Volume XIV, Issue XII, December 2025

over 60 weeks. The susceptible population declines gradually as individuals move to the exposed and infectious classes. Both symptomatic and asymptomatic infections remain relatively low due to intervention effects, while the recovered class increases sharply after week 40, approaching a steady state. The hesitant compartment remains nearly constant, reflecting behavioral inertia in vaccine acceptance. This persistence of hesitancy emphasizes the importance of sustained health education and trust-building measures to enhance immunization uptake, consistent with recent behavioral modeling studies [30]. Figure 6 (C), shows the temporal pattern of environmental bacterial concentration, $W_\tau(t)$, across different interventions. Under the baseline and environmental-only scenarios, pathogen levels increase and remain high, indicating ongoing environmental contamination. Conversely, vaccination and campaign strategies indirectly lower $W_\tau(t)$by reducing infectious hosts, while the combined intervention achieves the sharpest decline, confirming that simultaneous reduction in host infectivity and environmental shedding yields optimal results. This outcome echoes earlier findings that environmental disinfection complements medical control measures by shortening pathogen persistence [18]. Figure 6 (D), quantifies the percentage reduction in cumulative infections compared to the baseline. The reductions achieved are 98.3%, 97.7%, 97.4%, and 98.8% for vaccination, campaign, environmental, and combined interventions, respectively, whereas the baseline achieves only 35.9%. The combined control strategy, therefore, provides the most significant suppression of diphtheria transmission. The near-complete reduction demonstrates that combined, multi-level interventions, particularly vaccination coupled with intensive health campaigns, represent the most cost-effective and sustainable approach for epidemic management in resource-limited settings.

Moreover, Figure 6 (E), displays the relationship between the final outbreak size (recovered population) and the basic reproduction number, $R_0$, across different control strategies. The vertical dashed line marks the epidemic threshold ($\mathcal{R}_0 = 1$). All intervention scenarios yield $\mathcal{R}_0 < 1$, implying successful containment and convergence toward the disease-free equilibrium. The combined strategy leads to the smallest outbreak size, confirming theoretical expectations from the stability analysis presented in Section 3. This agrees with the well-established epidemiological principle that maintaining $\mathcal{R}_0 < 1$ensures infection eradication in the long term [39]. Figure 6 (F), depicts the temporal variation in the force of infection. Initially low, the infection pressure rises gradually during the early phase of the epidemic due to the accumulation of exposed individuals, then stabilizes and declines as interventions intensify. The eventual plateau reflects the progressive exhaustion of the susceptible and the efficacy of combined control measures. This declining pattern validates the effectiveness of integrated control programs in reducing disease transmissibility and curtailing epidemic potential.

In conclusion, the collective findings confirm that vaccination and public enlightenment campaigns are the most influential individual interventions for diphtheria control. However, when all interventions, vaccination, environmental sanitation, and public campaigns are applied together, the impact is synergistic, leading to dramatic reductions in infections, environmental contamination, and outbreak size. This emphasizes the necessity of comprehensive, coordinated approaches rather than isolated efforts.

**Formulation of Caputo-Fabrizio Fractional Model and Analysis**

Here, we extend the integer-order ordinary differential equation (ODE) to its corresponding non-integer-order fractional differential equation (FDE) model via the Caputo-Fabrizio fractional order derivative, which can sufficiently account for memory as well as nonlocal properties, allowing it to accommodate all points within the interval. Thus, replacing the first-order time derivatives of the left-hand side of (1) with the fractional Caputo-Fabrizio derivative, we obtain our new fractional differential equations (non-integer-order derivatives) as follows:

$$cF_{D_t^\alpha} S_\tau = \Pi + \omega V_\tau + \pi H_\tau - (\lambda_\tau + \delta + \xi + \mu) S_\tau$$

$$cF_{D_t^\alpha} E_\tau = \lambda_\tau S_\tau - (\sigma + \mu) E_\tau$$

$$cF_{D_t^\alpha} I_\tau = \sigma \varsigma E_\tau - (\gamma_1 + \phi_1 + \mu) I_\tau$$

$$cF_{D_t^\alpha} A_\tau = \sigma(1 - \varsigma) E_\tau - (\gamma_2 + \phi_2 + \mu) A_\tau$$

ISSN 2278-2540 | DOI: 10.51583/IJLTEMAS | Volume XIV, Issue XII, December 2025

$$cF_{D_t^{\alpha}}R_\tau = \gamma_1 I_\tau + \gamma_2 A_\tau - \mu R_\tau \quad (16)$$

$$cF_{D_t^{\alpha}}V_\tau = \delta S_\tau - (\omega + \mu)V_\tau$$

$$cF_{D_t^{\alpha}}H_\tau = \xi S_\tau - (\pi + \mu)H_\tau$$

$$cF_{D_t^{\alpha}}W_\tau = \varphi_1 I_\tau + \varphi_2 A_\tau - \vartheta W_\tau$$

where $cF_{D_t^{\alpha}}$represents the Caputo-Fabrizio fractional derivative of order $0 < \alpha \leq 1$, with the non-negative initial conditions

$$S_\tau(0) = S_{\tau_0}, E_\tau(0) = E_{\tau_0}, I_\tau(0) = I_{\tau_0}, A_\tau(0) = A_{\tau_0}, R_\tau(0) = R_{\tau_0}, V_\tau(0) = V_{\tau_0},$$

$$H_\tau(0) = H_{\tau_0}, W_\tau(0) = W_{\tau_0} \quad (17)$$

**Existence and Uniqueness of Solutions of The Model**

To evaluate and prove the existence and uniqueness of solutions to the Caputo-Fabrizio fractional model (16) for the dynamics of the diphtheria disease, with initial conditions (17), we use fixed-point theory as in ([17, 23]).

Applying the Caputo-Fabrizio fractional integral operator on both sides of (1), we have

$$S_\tau(t) - S_\tau(0) = cF_{I_t^{\alpha}}[\Pi + \omega V_\tau + \pi H_\tau - (\lambda_\tau + \delta + \xi + \mu)S_\tau],$$

$$E_\tau(t) - E_\tau(0) = cF_{I_t^{\alpha}}[\lambda_\tau S_\tau - (\sigma + \mu)E_\tau],$$

$$I_\tau(t) - I_\tau(0) = cF_{I_t^{\alpha}}[\sigma\varsigma E_\tau - (\gamma_1 + \phi_1 + \mu)I_\tau],$$

$$A_\tau(t) - A_\tau(0) = cF_{I_t^{\alpha}}[\sigma(1-\varsigma)E_\tau - (\gamma_2 + \phi_2 + \mu)A_\tau],$$

$$R_\tau(t) - R_\tau(0) = cF_{I_t^{\alpha}}[\gamma_1 I_\tau + \gamma_2 A_\tau - \mu R_\tau], \quad (18)$$

$$V_\tau(t) - V_\tau(0) = cF_{I_t^{\alpha}}[\delta S_\tau - (\omega + \mu)V_\tau]$$

$$H_\tau(t) - H_\tau(0) = cF_{I_t^{\alpha}}[\xi S_\tau - (\pi + \mu)H_\tau],$$

$$W_\tau(t) - W_\tau(0) = cF_{I_t^{\alpha}}[\varphi_1 I_\tau + \varphi_2 A_\tau - \vartheta W_\tau],$$

Then, the kernels of the system (16) can be written as follows

$$K_1(t, S_\tau) = \Pi + \omega V_\tau(t) + \pi H_\tau(t) - (\lambda_\tau + \delta + \xi + \mu)S_\tau(t)$$

$$K_2(t, E_\tau) = \lambda_\tau S_\tau(t) - (\sigma + \mu)E_\tau(t)$$

$$K_3(t, I_\tau) = \sigma\varsigma E_\tau(t) - (\gamma_1 + \phi_1 + \mu)I_\tau(t)$$

$$K_4(t, A_\tau) = \sigma(1-\varsigma)E_\tau(t) - (\gamma_2 + \phi_2 + \mu)A_\tau(t)$$

$$K_5(t, R_\tau) = \gamma_1 I_\tau(t) + \gamma_2 A_\tau(t) - \mu R_\tau(t) \quad (19)$$

$$K_6(t, V_\tau) = \delta S_\tau(t) - (\omega + \mu)V_\tau(t)$$

$$K_7(t, H_\tau) = \xi S_\tau(t) - (\pi + \mu)H_\tau(t)$$

$$K_8(t, W_\tau) = \varphi_1 I_\tau(t) + \varphi_2 A_\tau(t) - \vartheta W_\tau(t)$$

ISSN 2278-2540 | DOI: 10.51583/IJLTEMAS | Volume XIV, Issue XII, December 2025

And the functions $\Xi(\alpha) = \frac{2(1-\rho)}{(2-\rho)M(\rho)}$ and $\Theta(\alpha) = \frac{2\rho}{(2-\rho)M(\rho)}$ (20)

Thus, we assume that $S_\tau, E_\tau, I_\tau, A_\tau, R_\tau, V_\tau, H_\tau,$ and $W_\tau$ and are nonnegative bounded functions, when proving the following theorems, i.e.,

$$\|S_\tau(t)\| \le \theta_1, \|E_\tau(t)\| \le \theta_2, \|I_\tau(t)\| \le \theta_3, \|A_\tau(t)\| \le \theta_4,$$

$$\|R_\tau(t)\| \le \theta_5, \|V_\tau(t)\| \le \theta_6, \|H_\tau(t)\| \le \theta_7 \text{ and } \|W_\tau(t)\| \le \theta_8$$

where $\theta_1, \theta_2, \theta_3, \theta_4, \theta_5, \theta_6, \theta_7$ and $\theta_8$ are some positive constants.

Now let

$\Delta_1 = \lambda_\tau + \delta + \xi + \mu, \Delta_2 = \sigma + \mu, \Delta_3 = \gamma_1 + \phi_1 + \mu, \Delta_4 = \gamma_2 + \phi_2 + \mu, \Delta_5 = \mu, \Delta_6 = \omega + \mu, \Delta_7 = \pi + \mu$ and $\Delta_8 = \vartheta$ (21)

Applying the definition of the Caput-Fabrizio fractional integral operator in (18), we have.

$$S_\tau(t) - S_\tau(0) = \Xi(\alpha)K_1(t, S_\tau) + \Theta(\alpha)\int_0^t K_1(y, S_\tau)dy,$$

$$E_\tau(t) - E_\tau(0) = \Xi(\alpha)K_2(t, E_\tau) + \Theta(\alpha)\int_0^t K_2(y, E_\tau)dy,$$

$$I_\tau(t) - I_\tau(0) = \Xi(\alpha)K_3(t, I_\tau) + \Theta(\alpha)\int_0^t K_3(y, I_\tau)dy,$$

$$A_\tau(t) - A_\tau(0) = \Xi(\alpha)K_4(t, A_\tau) + \Theta(\alpha)\int_0^t K_4(y, A_\tau)dy,$$

$$R_\tau(t) - R_\tau(0) = \Xi(\alpha)K_5(t, R_\tau) + \Theta(\alpha)\int_0^t K_5(y, R_\tau)dy, \quad (22)$$

$$V_\tau(t) - V_\tau(0) = \Xi(\alpha)K_6(t, V_\tau) + \Theta(\alpha)\int_0^t K_6(y, V_\tau)dy$$

$$H_\tau(t) - H_\tau(0) = \Xi(\alpha)K_7(t, H_\tau) + \Theta(\alpha)\int_0^t K_7(y, H_\tau)dy,$$

$$W_\tau(t) - W_\tau(0) = \Xi(\alpha)K_8(t, W_\tau) + \Theta(\alpha)\int_0^t K_8(y, W_\tau)dy,$$

**Theorem 6**: If the following inequality holds

$$0 \le M = \max\{\Delta_1, \Delta_2, \Delta_3, \Delta_4, \Delta_5, \Delta_6, \Delta_7, \Delta_8\} < 1, \quad (23)$$

Then the kernels $K_1, K_2, K_3, K_4, K_5, K_6, K_7$ and $K_8$ satisfy Lipschitz conditions and are contraction mappings.

**Proof.** We consider the kernel $K_1$. Let $S_\tau$ and $S_{\tau_1}$ be any two functions, then we have

$$\left\|K_1(t, S_\tau) - K_1\left(t, S_{\tau_I}\right)\right\| = \left\|-\lambda_\tau\left(S_\tau(t) - S_{\tau_1}(t)\right) - \delta\left(S_\tau(t) - S_{\tau_1}(t)\right) - \xi\left(S_\tau(t) - S_{\tau_1}(t)\right) - \mu\left(S_\tau(t) - S_{\tau_1}(t)\right)\right\| \quad (24)$$

Using the triangle inequality for norms on the right-hand side of (24), we have

$$\begin{aligned}\left\|K_1(t, S_\tau) - K_1\left(t, S_{\tau_I}\right)\right\| &\le \left\|\lambda_\tau\left(S_\tau(t) - S_{\tau_1}(t)\right)\right\| + \left\|\delta\left(S_\tau(t) - S_{\tau_1}(t)\right)\right\| + \left\|\xi\left(S_\tau(t) - S_{\tau_1}(t)\right)\right\| \\ &+ \left\|\mu\left(S_\tau(t) - S_{\tau_1}(t)\right)\right\|\end{aligned}$$

ISSN 2278-2540 | DOI: 10.51583/IJLTEMAS | Volume XIV, Issue XII, December 2025

$$\leq (\lambda_\tau + \delta + \xi + \mu)\left\|S_\tau(t) - S_{\tau_1}(t)\right\|$$

$$\leq (\lambda_\tau + \delta + \xi + \mu)\left\|S_\tau(t) - S_{\tau_1}(t)\right\|$$

$$= \Delta_1\left\|S_\tau(t) - S_{\tau_1}(t)\right\|.$$

Where $\Delta_1$ is as defined in (21). Comparable outcomes for the kernels $K_2, K_3, K_4, K_5, K_6, K_7$ and $K_8$ can be obtained using $\{E_\tau, E_{\tau_1}\}$,$\{I_\tau, I_{\tau_1}\}$,$\{A_\tau, A_{\tau_1}\}$,$\{R_\tau, R_{\tau_1}\}$,$\{V_\tau, V_{\tau_1}\}$,$\{H_\tau, H_{\tau_1}\}$ and $\{W_\tau, W_{\tau_1}\}$, respectively, as follows:

$$\left\|K_2(t, E_\tau) - K_2\left(t, E_{\tau_l}\right)\right\| \leq \Delta_2\left\|E_\tau(t) - E_{\tau_1}(t)\right\|$$

$$\left\|K_3(t, I_\tau) - K_3\left(t, I_{\tau_1}\right)\right\| \leq \Delta_3\left\|I_\tau(t) - I_{\tau_1}(t)\right\|$$

$$\left\|K_4(t, A_\tau) - K_4\left(t, A_{\tau_1}\right)\right\| \leq \Delta_4\left\|A_\tau(t) - A_{\tau_1}(t)\right\|$$

$$\left\|K_5(t, R_\tau) - K_5\left(t, R_{\tau_l}\right)\right\| \leq \Delta_5\left\|R_\tau(t) - R_{\tau_1}(t)\right\|$$

$$\left\|K_6(t, V_\tau) - K_6\left(t, V_{\tau_l}\right)\right\| \leq \Delta_6\left\|V_\tau(t) - V_{\tau_1}(t)\right\| \qquad (25)$$

$$\left\|K_7(t, H_\tau) - K_7\left(t, H_{\tau_1}\right)\right\| \leq \Delta_7\left\|H_\tau(t) - H_{\tau_1}(t)\right\|$$

$$\left\|K_8(t, W) - K_8\left(t, W_{\tau_1}\right)\right\| \leq \Delta_8\left\|W(t) - W_{\tau_1}(t)\right\|$$

where $\Delta_1, \Delta_2, \Delta_3, \Delta_4, \Delta_5, \Delta_6, \Delta_7$ and $\Delta_8$ are defined in (21).

Therefore, the Lipschitz conditions are satisfied for $K_2, K_3, K_4, K_5, K_6, K_7$ and $K_8$. In addition, since $0 \leq M = \max\{\Delta_1, \Delta_2, \Delta_3, \Delta_4, \Delta_5, \Delta_6, \Delta_7, \Delta_8\} < 1$,

the kernels are contractions. From (22), the state variables can be displayed in terms of the kernels as follows:

$$S_\tau(t) = S_\tau(0) + \Xi(\alpha)K_1(t, S_\tau) + \Theta(\alpha)\int_0^t K_1(y, S_\tau)dy,$$

$$E_\tau(t) = E_\tau(0) + \Xi(\alpha)K_2(t, E_\tau) + \Theta(\alpha)\int_0^t K_2(y, E_\tau)dy,$$

$$I_\tau(t) = I_\tau(0) + \Xi(\alpha)K_3(t, I_\tau) + \Theta(\alpha)\int_0^t K_3(y, I_\tau)dy,$$

$$A_\tau(t) = A_\tau(0) + \Xi(\alpha)K_4(t, A_\tau) + \Theta(\alpha)\int_0^t K_4(y, A_\tau)dy,$$

$$R_\tau(t) = R_\tau(0) + \Xi(\alpha)K_5(t, R_\tau) + \Theta(\alpha)\int_0^t K_5(y, R_\tau)dy, \qquad (26)$$

$$V_\tau(t) = V_\tau(0) + \Xi(\alpha)K_6(t, V_\tau) + \Theta(\alpha)\int_0^t K_6(y, V_\tau)dy$$

$$H_\tau(t) = (0) + \Xi(\alpha)K_7(t, H_\tau) + \Theta(\alpha)\int_0^t K_7(y, H_\tau)dy,$$

$$W_\tau(t) = W_\tau(0) + \Xi(\alpha)K_8(t, W_\tau) + \Theta(\alpha)\int_0^t K_8(y, W_\tau)dy,$$

Using (26), we now introduce the following recursive formulas:

$$S_{\tau_n}(t) = \Xi(\alpha)K_1\left(t, S_{\tau_{n-1}}\right) + \Theta(\alpha)\int_0^t K_1\left(y, S_{\tau_{n-1}}\right)dy,$$

ISSN 2278-2540 | DOI: 10.51583/IJLTEMAS | Volume XIV, Issue XII, December 2025

$$E_{\tau_n}(t) = \Xi(\alpha)K_2\left(t, E_{\tau_{n-1}}\right) + \Theta(\alpha)\int_0^t K_2\left(y, E_{\tau_{n-1}}\right)dy,$$

$$I_{\tau_n}(t) = \Xi(\alpha)K_3\left(t, I_{\tau_{(n-1)}}\right) + \Theta(\alpha)\int_0^t K_3\left(y, I_{\tau_{(n-1)}}\right)dy,$$

$$A_{\tau_n}(t) = \Xi(\alpha)K_4\left(t, A_{\tau_{(n-1)}}\right) + \Theta(\alpha)\int_0^t K_4\left(y, A_{\tau_{(n-1)}}\right)dy, \quad (27)$$

$$R_{\tau_n}(t) = \Xi(\alpha)K_5\left(t, R_{\tau_{n-1}}\right) + \Theta(\alpha)\int_0^t K_5\left(y, R_{\tau_{n-1}}\right)dy,$$

$$V_{\tau_n}(t) = \Xi(\alpha)K_6\left(t, V_{\tau_{n-1}}\right) + \Theta(\alpha)\int_0^t K_6\left(y, V_{\tau_{(n-1)}}\right)dy$$

$$H_{\tau_n}(t) = \Xi(\alpha)K_7\left(t, H_{\tau_{(n-1)}}\right) + \Theta(\alpha)\int_0^t K_7\left(y, H_{\tau_{(n-1)}}\right)dy,$$

$$W_{\tau_n}(t) = \Xi(\alpha)K_8\left(t, W_{\tau_{(n-1)}}\right) + \Theta(\alpha)\int_0^t K_8\left(y, W_{\tau_{(n-1)}}\right)dy.$$

The initial components of the above recursive formulas are determined by the following initial conditions:

$$S_{\tau_0}(t) = S_\tau(0), E_{\tau_0}(t) = E_\tau(0), I_{\tau_0}(t) = I_\tau(0), A_{\tau_0}(t) = A_\tau(0), R_{\tau_0}(t) = R_\tau(0),$$

$$V_{\tau_0}(t) = V_\tau(0), H_{\tau_0}(t) = H_\tau(0), W_{\tau_0}(t) = W_\tau(0) \quad (28)$$

Hence, the differences between the consecutive terms for the recursive formulas can be written as

$$\Upsilon_{1n}(t) = S_{\tau_n}(t) - S_{\tau_{n-1}}(t) = \Xi(\alpha)(K_1\left(t, S_{\tau_{n-1}}\right) - K_1\left(t, S_{\tau_{n-2}}\right))$$

$$+\Theta(\alpha)\int_0^t (K_1\left(y, S_{\tau_{n-1}} - K_1\left(t, S_{\tau_{n-2}}\right)\right)dy,$$

$$\Upsilon_{2n}(t) = E_{\tau_n}(t) - E_{\tau_{n-1}}(t) = \Xi(\alpha)(K_2\left(t, E_{\tau_{n-1}}\right) - K_2\left(t, E_{\tau_{n-2}}\right))$$

$$+\Theta(\alpha)\int_0^t (K_2\left(y, E_{\tau_{n-1}} - K_2\left(t, E_{\tau_{n-2}}\right)\right)dy$$

$$\Upsilon_{3n}(t) = I_{\tau_n}(t) - I_{\tau_{n-1}} = \Xi(\alpha)(K_3\left(t, I_{\tau_{n-1}}\right) - K_3\left(t, I_{\tau_{n-2}}\right))$$

$$+\Theta(\alpha)\int_0^t (K_3\left(y, I_{\tau_{n-1}} - K_3\left(t, I_{\tau_{n-2}}\right)\right)dy,$$

$$\Upsilon_{4n}(t) = A_{\tau_n}(t) - A_{\tau_{n-1}}(t) = \Xi(\alpha)(K_4\left(t, A_{\tau_{n-1}}\right) - K_4\left(t, A_{\tau_{n-2}}\right))$$

$$+\Theta(\alpha)\int_0^t (K_4\left(y, A_{\tau_{n-1}} - K_4\left(t, A_{\tau_{n-2}}\right)\right)dy,$$

$$\Upsilon_{5n}(t) = R_{\tau_n}(t) - R_{\tau_{n-1}}(t) = \Xi(\alpha)(K_5\left(t, R_{\tau_{n-1}}\right) - K_5\left(t, R_{\tau_{n-2}}\right)) \quad (29)$$

$$+\Theta(\alpha)\int_0^t (K_5\left(y, R_{\tau_{n-1}} - K_5\left(t, R_{\tau_{n-2}}\right)\right)dy,$$

$$\Upsilon_{6n}(t) = V_{\tau_n}(t) - V_{\tau_{n-1}}(t) = \Xi(\alpha)(K_6\left(t, V_{\tau_{n-1}}\right) - K_6\left(t, V_{\tau_{n-2}}\right))$$

$$+\Theta(\alpha)\int_0^t (K_6\left(y, V_{\tau_{n-1}} - K_6\left(t, V_{\tau_{n-2}}\right)\right)dy,$$

ISSN 2278-2540 | DOI: 10.51583/IJLTEMAS | Volume XIV, Issue XII, December 2025

$$\Upsilon_{7n}(t) = H_{\tau_n}(t) - H_{\tau_{n-1}}(t) = \Xi(\alpha)(K_7(t, H_{\tau_{n-1}}) - K_7(t, H_{\tau_{n-2}}))$$

$$+\Theta(\alpha)\int_0^t (K_7\left(y, H_{\tau_{n-1}} - K_7(t, H_{\tau_{n-2}})\right) dy,$$

$$\Upsilon_{8n}(t) = W_{\tau_n}(t) - W_{\tau_{n-1}}(t) = \Xi(\alpha)(K_8(t, W_{\tau_{n-1}}) - K_8(t, W_{\tau_{n-2}}))$$

$$+\Theta(\alpha)\int_0^t (K_8\left(y, W_{\tau_{n-1}} - K_8(t, W_{\tau_{n-2}})\right) dy,$$

For $S_{\tau_n}(t) = \sum_{i=1}^{n} \Upsilon_{1i}(t), E_n(t) = \sum_{i=1}^{n} \Upsilon_{2i}(t), I_{\tau_n}(t) = \sum_{i=1}^{n} \Upsilon_{3i}(t), A_{\tau_n}(t) = \sum_{i=1}^{n} \Upsilon_{4i}(t)$

$, R_{\tau_n}(t) = \sum_{i=1}^{n} \Upsilon_{5n_i}(t), V_{\tau_n}(t) = \sum_{i=1}^{n} \Upsilon_{6i}(t), H_{\tau_n}(t) = \sum_{i=1}^{n} \Upsilon_{7i}(t), W_{\tau_n}(t) = \sum_{i=1}^{n} \Upsilon_{8i}(t)$ (30)

Now, let's generate the recursive inequalities for the differences $\Upsilon_{1n}, \Upsilon_{2n}, \Upsilon_{3n}, \Upsilon_{4n}, \Upsilon_{5n}, \Upsilon_{6n}, \Upsilon_{7n}$ and $\Upsilon_{8n}$ as follows

$$\|\Upsilon_{1n}(t)\| = \left\|S_{\tau_n}(t) - S_{\tau_{n-1}}(t)\right\| = \left\|\Xi(\alpha)(K_1(t, S_{\tau_{n-1}}) - K_1(t, S_{\tau_{n-2}})) + \Theta(\alpha)\int_0^t (K_1\left(y, S_{\tau_{n-1}} - K_1(t, S_{\tau_{n-2}})\right) dy\right\| \quad (31)$$

Using the triangle inequality for norms to (31), we have

$$\left\|S_{\tau_n}(t) - S_{\tau_{n-1}}(t)\right\| = \left\|\Xi(\alpha) \Vdash K_1(t, S_{\tau_{n-1}}) - K_1(t, S_{\tau_{n-2}})\right\|$$

$$+ \Theta(\alpha)\int_0^t \left\|K_1(y, S_{\tau_{n-1}}) - K_1(t, S_{\tau_{n-2}})\right\| dy$$

Then, since the kernel $K_1$ satisfies the Lipschitz condition with Lipschitz constant $\Delta_1$, we have

$$\left\|S_{\tau_n}(t) - S_{\tau_{n-1}}(t)\right\| \leq \left\|\Xi(\alpha)\Delta_1 \Vdash S_{\tau_{n-1}} - S_{\tau_{n-2}}\right\| + \Theta(\alpha)\Delta_1 \int_0^t \left\|S_{\tau_{n-1}} - S_{\tau_{n-2}}\right\| dy$$

therefore, $\|\Upsilon_{1n}(t)\| \leq \Xi(\alpha)\Delta_1\left\|\Upsilon_{1(n-1)}(t)\right\| + \Theta(\alpha)\Delta_1 \int_0^t \left\|\Upsilon_{1(n-1)}(y)\right\| dy$ (32)

Following the same procedures, we have

$$\|\Upsilon_{2n}(t)\| \leq \Xi(\alpha)\Delta_2\left\|\Upsilon_{2(n-1)}(t)\right\| + \Theta(\alpha)\Delta_2 \int_0^t \left\|\Upsilon_{2(n-1)}(y)\right\| dy$$

$$\|\Upsilon_{3n}(t)\| \leq \Xi(\alpha)\Delta_3\left\|\Upsilon_{3(n-1)}(t)\right\| + \Theta(\alpha)\Delta_3 \int_0^t \left\|\Upsilon_{3(n-1)}(y)\right\| dy \qquad \|\Upsilon_{4n}(t)\| \leq \Xi(\alpha)\Delta_4\left\|\Upsilon_{4(n-1)}(t)\right\| + \Theta(\alpha)\Delta_4 \int_0^t \left\|\Upsilon_{4(n-1)}(y)\right\| dy$$

$$\|\Upsilon_{5n}(t)\| \leq \Xi(\alpha)\Delta_5\left\|\Upsilon_{5(n-1)}(t)\right\| + \Theta(\alpha)\Delta_5 \int_0^t \left\|\Upsilon_{5(n-1)}(y)\right\| dy \quad (33)$$

$$\|\Upsilon_{6n}(t)\| \leq \Xi(\alpha)\aleph_6\left\|\Upsilon_{6(n-1)}(t)\right\| + \Theta(\alpha)\Delta_6 \int_0^t \left\|\Upsilon_{6(n-1)}(y)\right\| dy$$

$$\|\Upsilon_{7n}(t)\| \leq \Xi(\alpha)\Delta_7\left\|\Upsilon_{7(n-1)}(t)\right\| + \Theta(\alpha)\Delta_7 \int_0^t \left\|\Upsilon_{7(n-1)}(y)\right\| dy$$

$$\|\Upsilon_{8n}(t)\| \leq \Xi(\alpha)\Delta_8\left\|\Upsilon_{8(n-1)}(t)\right\| + \Theta(\alpha)\Delta_8 \int_0^t \left\|\Upsilon_{8(n-1)}(y)\right\| dy$$

**Theorem 7:** If there exists a time $t_0 > 0$ such that the following inequalities hold:

$$\Xi(\alpha)\Delta_i + \Theta(\alpha)\,\Delta_i t_0 > 1, \text{ for } i = 1,2,\ldots,8, \quad (34)$$

ISSN 2278-2540 | DOI: 10.51583/IJLTEMAS | Volume XIV, Issue XII, December 2025

then the solution exists for the fractional diphtheria model (16) with (17).

**Proof.** Assuming the functions$S_\tau, E_\tau, I_\tau, A_\tau, R_\tau, V_\tau, H_\tau,\ and\ W_\tau$ are bounded and each of the kernels satisfies a Lipschitz condition, then the following relations can be obtained.

Using $(33)-(34)$ recursively:

$$\|\Upsilon_{1n}(t)\| \le \|S_\tau(0)\|[\Xi(\alpha)\Delta_1 + \Theta(\alpha)\Delta_1]^n$$

$$\|\Upsilon_{2n}(t)\| \le \|E_\tau(0)\|\,[\Xi(\alpha)\Delta_2 + \Theta(\alpha)\Delta_2]^n$$

$$\|\Upsilon_{3n}(t)\| \le \|I_\tau(0)\|[\Xi(\alpha)\Delta_3 + \Theta(\alpha)\Delta_3]^n$$

$$\|\Upsilon_{4n}(t)\| \le \|A_\tau(0)\|[\Xi(\alpha)\Delta_4 + \Theta(\alpha)\Delta_4]^n$$

$$\|\Upsilon_{5n}(t)\| \le \|R_\tau(0)\|[\Xi(\alpha)\Delta_5 + \Theta(\alpha)\Delta_5]^n \qquad (35)$$

$$\|\Upsilon_{6n}(t)\| \le \|V_\tau(0)\|[\Xi(\alpha)\Delta_6 + \Theta(\alpha)\Delta_6]^n$$

$$\|\Upsilon_{7n}(t)\| \le \|H_\tau(0)\|[\Xi(\alpha)\Delta_7 + \Theta(\alpha)\Delta_7]^n$$

$$\|\Upsilon_{8n}(t)\| \le \|W_\tau(0)\|[\Xi(\alpha)\Delta_8 + \Theta(\alpha)\Delta_8]^n$$

Equation (35) shows the existence and smoothness of the functions defined in (31).

To complete the proof, we prove that the functions $S_{\tau_n}(t), E_{\tau_n}(t), I_{\tau_n}(t), A_{\tau_n}(t), R_{\tau_n}(t), V_{\tau_n}(t), H_{\tau_n}$ and $W_{\tau_n}(t)$ converge to a solution of $(16)\ with\ (17)$.

We introduce $B_{1n}(t)$, $B_{2n}(t), B_{3n}(t)$, $B_{4n}(t)$, $B_{5n}(t), B_{6n}(t)$, $B_{7n}(t)$ and $B_{8n}(t)$, as the remainder terms after $n$ iteration, so that

$$S_\tau(t) - S_\tau(0) = S_{\tau_n}(t) - B_{1n}(t),$$

$$E_\tau(t) - E_\tau(0) = E_{\tau_n}(t) - B_{2n}(t),,$$

$$I_\tau(t) - I_\tau(0) = I_{\tau_n}(t) - B_{3n}(t),$$

$$A_\tau(t) - A_\tau(0) = A_{\tau_n}(t) - B_{4n}(t),$$

$$R_\tau(t) - R_\tau(0) = R_{\tau_n}(t) - B_{5n}(t), \qquad (36)$$

$$V_\tau(t) - V_\tau(0) = V_{\tau_n}(t) - B_{6n}(t),$$

$$H_\tau(t) - H_\tau(0) = H_{\tau_n}(t) - B_{7n}(t),$$

$$W_\tau(t) - W_\tau(0) = W_{\tau_n}(t) - B_{8n}(t),$$

Then, using the triangle inequality and the Lipschitz condition for $K_1$, we have

$$\|B_{1n}(t)\| = \left\|\Xi(\alpha)(K_1(t,S_\tau) - K_1\left(t,S_{\tau_{n-1)}}\right)) + \Theta(\alpha)\int_0^t (K_1(y,S_\tau) - K_1(y,S_{\tau_{n-1}}))dy\right\|$$

$$\le \Xi(\alpha)\left\|(K_1(t,S_\tau) - K_1\left(t,S_{\tau_{n-1}}\right)\right\| + \Theta(\alpha)\int_0^t \left\|K_1(y,S_\tau) - K_1(y,S_{\tau_{n-1}})\right\|dy$$

ISSN 2278-2540 | DOI: 10.51583/IJLTEMAS | Volume XIV, Issue XII, December 2025

$$\leq \Xi(\alpha)\Delta_1\|S_\tau - S_{\tau_{n-1}}\| + \Theta(\alpha)\Delta_1 B_{1n}(t)\|S_\tau - S_{\tau_{n-1}}\|t.$$

Repeating the same process, we have;

$$\|B_{1n}(t)\| \leq [(\Xi(\alpha) + \Theta(\alpha)t)\Delta_1]^{n+1}\theta_1 \quad (37)$$

At $t_0$ we have

$$\|B_{1n}(t)\| \leq [(\Xi(\alpha) + \Theta(\alpha)t_0)\Delta_1]^{n+1}\theta_1 \quad (38)$$

Taking the limit on (38) as $n \to \infty$ and then using the condition (34), we obtain $\|B_{1n}(t)\| \to 0$. Using the same process as described above, we have the following relations:

$$\|B_{2n}(t)\| \leq [(\Xi(\alpha) + \Theta(\alpha)t_0)\Delta_2]^{n+1}\theta_2 \quad \|B_{3n}(t)\| \leq [(\Xi(\alpha) + \Theta(\alpha)t_0)\Delta_3]^{n+1}\theta_3 \quad \|B_{4n}(t)\| \leq [(\Xi(\alpha) + \Theta(\alpha)t_0)\Delta_4]^{n+1}\theta_4 \quad \|B_{5n}(t)\| \leq [(\Xi(\alpha) + \Theta(\alpha)t_0)\Delta_5]^{n+1}\theta_5 \quad (40)$$

$$\|B_{6n}(t)\| \leq [(\Xi(\alpha) + \Theta(\alpha)t_0)\Delta_6]^{n+1}\theta_6$$

$$\|B_{7n}(t)\| \leq [(\Xi(\alpha) + \Theta(\alpha)t_0)\Delta_7]^{n+1}\theta_7$$

$$\|B_{8n}(t)\| \leq [(\Xi(\alpha) + \Theta(\alpha)t_0)\Delta_8]^{n+1}\theta_8$$

Similarly, taking the limit on (39) as $n \to \infty$ and then using the condition (34), we have $\|B_{2n}(t)\| \to 0, \|B_{3n}(t)\| \to 0, \|B_{4n}(t)\| \to 0, \|B_{5n}(t)\| \to 0, \|B_{6n}(t)\| \to 0, \|B_{7n}(t)\| \to 0$ and $\|B_{8n}(t)\| \to 0$. Therefore, the existence of solutions of the model system (16) with (17) is proved.

We now consider the following conditions for the system of solutions to be unique.

**Theorem 8:** System (16) along with the initial conditions (17) has a unique solution if the following conditions hold: $(1 - \Xi(\alpha)\Delta_i + \Theta(\alpha)\Delta_i t > 0)$, for $i = 1,2,\ldots,8$. (40)

**Proof.** Assume that $\{S_{\tau_n}(t), E_{\tau_n}(t), I_{\tau_n}(t), A_{\tau_n}(t), R_{\tau_n}(t), V_{\tau_n}(t), H_{\tau_n}$ and $W_{\tau_n}(t)\}$ is another set of solutions for the model (16) with (17) in addition to the solution set $\{S_{\tau_n}(t), E_{\tau_n}(t), I_{\tau_n}(t), A_{\tau_n}(t), R_{\tau_n}(t), V_{\tau_n}(t), H_{\tau_n}$ and $W_{\tau_n}(t)\}$ proved to exist in Theorems 6 and 7, then

$$S_\tau(t) - S_{\tau_1}(t) = \Xi(\alpha)(K_1(t, S_\tau) - K_1(t, S_{\tau_1}) + \Theta(\alpha)\int_0^t (K_1(y, S_\tau) - K_1(y, S_{\tau_1}))dy \quad (41)$$

Taking the norm and triangle inequality on both sides of (41), we have

$$\|S_\tau(t) - S_{\tau_1}(t)\| \leq \Xi(\alpha)\|K_1(t, S_\tau) - K_1(t, S_{\tau_1})\| + \Theta(\alpha)\int_0^t \|(K_1(y, S_\tau) - K_1(y, S_{\tau_1})\| \quad (42)$$

Using the Lipschitz condition for the kernel $K_1$, we find

$$\|S_\tau(t) - S_{\tau_1}(t)\| \leq \Xi(\alpha)\Delta_1\|S(t) - S_{\tau_1}(t)\| + \Theta(\alpha)\Delta_1 t\|S_\tau(t) - S_{\tau_1}(t)\| \quad (43)$$

Rearranging (42), we have

$$\|S_\tau(t) - S_{\tau_1}(t)\|1 - \Xi(\alpha)\Delta_i + \Theta(\alpha)\Delta_i t \leq 0 \quad (44)$$

Lastly, putting in condition (42) for $i = 1$ to (44), we have

$$\|S_\tau(t) - S_{\tau_1}(t)\| = 0 \quad (45)$$

ISSN 2278-2540 | DOI: 10.51583/IJLTEMAS | Volume XIV, Issue XII, December 2025

Hence $S_\tau(t) = S_{\tau_1}(t)$. Now putting in a similar procedure to each of the following pairs

$(E_\tau(t), E_{\tau_1}(t)), (I_\tau(t), I_{\tau_1}(t)), (A_\tau(t), A_{\tau_1}(t)), (R_\tau(t), R_{\tau_1}(t))\ (V_\tau(t), V_{\tau_1}(t)), (H_\tau(t),\ H_{r_1}(t))$

and $(W_r(t),\ W_{r_1}(t))$ With inequality (42) for $i = 1,2,\ldots,8$, respectively, we have

$$(E_\tau(t) = E_{\tau_1}(t)), (I_\tau(t) = I_{\tau_1}(t)), (A_\tau(t) = A_{\tau_1}(t)), (R_\tau(t) = R_{\tau_1}(t)), (V_\tau(t) = V_{\tau_1}(t)), (H_\tau(t) = H_{r_1}(t)), \text{and } (W_r(t) = W_{r_1}(t)) \quad (46)$$

Thus, the uniqueness of the solutions of the fractional order system is proved.

**Adams-Bashforth-Moulton Scheme of the model system**

Several numerical techniques have been proposed to solve a wide range of nonlinear fractional-order derivative models arising in real-world problems. The analytical methods developed to handle these problems include Adomian Decomposition, finite difference, and the Homotopy Decomposition Method. Here, we use the Adams-Bashforth-Moulton method to provide an approximate solution for the model (1) based on the Predator-Corrector algorithm.

Thus, setting $h = \frac{T}{N}, t_n = nh\ and\ n = 0,1,2,\ldots \mathrm{N}\epsilon\mathbb{Z}^+$ as in ([6, 10]), then system (1) can be discretized using the approach of [12]. Now the corrector values are

$$S_{\tau_{n+1}} = S_{\tau_0} + \frac{h^\alpha}{\Gamma(\alpha+2)}\left[\Pi - \left((1-C\varepsilon)\left[\frac{\beta_1(I^p_{\tau(n+1)} + \theta A^p_{\tau(n+1)})}{N^p_{\tau(n+1)}} + \frac{\beta_2 W^p_{r(n+1)}}{\kappa + W^p_{r(n+1)}}\right] - \mu\right) S^p_{\tau_{n+1}} + \omega V^p_{\tau_{n+1}} + \pi H^p_{\tau_{n+1}} - (\delta + \xi + \mu) S^p_{\tau_{n+1}}\right] + \frac{h^\alpha}{\Gamma(\alpha+2)}\sum_{i=0}^{n} x_{i,n+1}\left[\Pi - \left((1-C\varepsilon)\left[\frac{\beta_1(I_{\tau_i} + \theta A_{\tau_i})}{N_{\tau_i}} + \frac{\beta_2 W_{\tau_i}}{\kappa + W_{\tau_i}}\right] - \mu\right) S_{\tau_i} + \omega V_{\tau_i} + \pi H_{\tau_i} - (\delta + \xi + \mu) S_{\tau_i}\right],$$

$$E_{\tau_{n+1}} = E_{\tau_0} + \frac{h^\alpha}{\Gamma(\alpha+2)}\left[\left((1-C\varepsilon)\left[\frac{\beta_1(I^p_{\tau(n+1)} + \theta A^p_{\tau(n+1)})}{N^p_{\tau(n+1)}} + \frac{\beta_2 W^p_{r(n+1)}}{\kappa + W^p_{r(n+1)}}\right]\right) S^p_{\tau_{n+1}} - (\sigma + \mu) E^p_{\tau_{n+1}}\right] + \frac{h^\alpha}{\Gamma(\alpha+2)}\sum_{i=0}^{n} x_{i,n+1}\left[\left((1-C\varepsilon)\left[\frac{\beta_1(I_{\tau_i} + \theta A_{\tau_i})}{N_{\tau_i}} + \frac{\beta_2 W_{\tau_i}}{\kappa + W_{\tau_i}}\right]\right) S_{\tau_i} - (\vartheta + \mu) E_{\tau_i}\right],$$

$$I_{\tau_{(n+1)}} = I_{\tau_0} + \frac{h^\alpha}{\Gamma(\alpha+2)}\left[\varsigma\sigma E^p_{\tau_{n+1}} - (\gamma_1 + \phi_1 + \mu) I^p_{\tau_{n+1}}\right] + \frac{h^\alpha}{\Gamma(\alpha+2)}\sum_{i=0}^{n} x_{i,n+1}\left[\varsigma\sigma E_{\tau_i} - (\gamma_1 + \phi_1 + \mu) I_{\tau_i}\right],$$

$$A_{\tau_{(n+1)}} = A_{\tau_0} + \frac{h^\alpha}{\Gamma(\alpha+2)}\left[\sigma(1-\varsigma) E^p_{\tau_{n+1}} - (\gamma_2 + \phi_2 + \mu) A^p_{\tau_{n+1}}\right] + \frac{h^\alpha}{\Gamma(\alpha+2)}\sum_{i=0}^{n} x_{i,n+1}\left[\sigma(1-\varsigma) E_{\tau_i} - (\gamma_2 + \phi_2 + \mu) A_{\tau_i}\right],$$

ISSN 2278-2540 | DOI: 10.51583/IJLTEMAS | Volume XIV, Issue XII, December 2025

$$R_{\tau_{n+1}} = R_{\tau_0} + \frac{h^\alpha}{\Gamma(\alpha+2)}\left[\gamma_1 I_{\tau_{n+1}}^{\,p} + \gamma_2 A_{\tau_{n+1}}^{\,p} - \mu R_{\tau_{n+1}}^{\,p}\right] + \frac{h^\alpha}{\Gamma(\alpha+2)}\sum_{i=0}^{n} x_{i,n+1}\left[\gamma_1 I_{\tau_i} + \gamma_2 A_{\tau_i} - \mu R_{\tau_i}\right],$$

$$V_{\tau_{n+1}} = V_{\tau_0} + \frac{h^\alpha}{\Gamma(\alpha+2)}\left[\delta S_{\tau_{n+1}}^{\,p} - (\omega+\mu) V_{\tau_{n+1}}^{\,p}\right] + \frac{h^\alpha}{\Gamma(\alpha+2)}\sum_{i=0}^{n} x_{i,n+1}\left[\delta S_{\tau_i} - (\omega+\mu) V_{\tau_i}\right],$$

$$H_{\tau_{n+1}} = H_{\tau_0} + \frac{h^\alpha}{\Gamma(\alpha+2)}\left[\xi S_{\tau_{n+1}}^{\,p} - (\pi+\mu) H_{\tau_{n+1}}^{\,p}\right] + \frac{h^\alpha}{\Gamma(\alpha+2)}\sum_{i=0}^{n} x_{i,n+1}\left[\xi S_{\tau_i} - (\pi+\mu) H_{\tau_i}\right]$$

$$W_{\tau_{n+1}} = W_{\tau_0} + \frac{h^\alpha}{\Gamma(\alpha+2)}\left[\varphi_1 I_{\tau_{n+1}}^{\,p} + \varphi_2 A_{\tau_{n+1}}^{\,p} - \vartheta W_{\tau_{n+1}}^{\,p}\right] + \frac{h^\alpha}{\Gamma(\alpha+2)}\sum_{i=0}^{n} x_{i,n+1}\left[\varphi_1 I_{\tau_i} + \varphi_2 A_{\tau_i} - \vartheta W_{\tau_i}\right],$$

Where

$$S_{\tau_{n+1}}^{\,p} = S_{\tau_0} + \frac{1}{\Gamma(\alpha)}\sum_{i=0}^{n} y_{i,n+1}\left[\Pi - \left((1-C\varepsilon)\left[\frac{\beta_1(I_{\tau_i}+\theta A_{\tau_i})}{N_{\tau_i}} + \frac{\beta_2 W_{\tau_i}}{\kappa + W_{\tau_i}}\right] - \mu\right) S_{\tau_i} + \omega V_{\tau_i} + \pi H_{\tau_i} - (\delta+\xi+\mu) S_{\tau_i}\right],$$

$$E_{\tau_{n+1}}^{\,p} = E_{\tau_0} + \frac{1}{\Gamma(\alpha)}\sum_{i=0}^{n} y_{i,n+1}\left[\left((1-C\varepsilon)\left[\frac{\beta_1(I_{\tau_i}+\theta A_{\tau_i})}{N_{\tau_i}} + \frac{\beta_2 W_{\tau_i}}{\kappa + W_{\tau_i}}\right]\right) S_{\tau_i} - (\vartheta+\mu) E_{\tau_i}\right],$$

$$I_{\tau_{n+1}}^{\,p} = I_{\tau_0} + \frac{1}{\Gamma(\alpha)}\sum_{i=0}^{n} y_{i,n+1}\left[\varsigma\sigma E_{\tau_i} - (\gamma_1 + \phi_1 + \mu) I_{\tau_i}\right],$$

$$A_{\tau_{n+1}}^{\,p} = A_{\tau_0} + \frac{1}{\Gamma(\alpha)}\sum_{i=0}^{n} y_{i,n+1}\left[\sigma(1-\varsigma) E_{\tau_i} - (\gamma_2 + \phi_2 + \mu) A_{\tau_i}\right],$$

$$R_{\tau_{n+1}}^{\,p} = R_{\tau_0} + \frac{1}{\Gamma(\alpha)}\sum_{i=0}^{n} y_{i,n+1}\left[\gamma_1 I_{\tau_i} + \gamma_2 A_{\tau_i} - \mu R_{\tau_i}\right],$$

$$V_{\tau_{n+1}}^{\,p} = V_{\tau_0} + \frac{1}{\Gamma(\alpha)}\sum_{i=0}^{n} y_{i,n+1}\left[\delta S_{\tau_i} - (\omega+\mu) V_{\tau_i}\right],$$

$$H_{\tau_{n+1}}^{\,p} = H_{\tau_0} + \frac{1}{\Gamma(\alpha)}\sum_{i=0}^{n} y_{i,n+1}\left[\xi S_{\tau_i} - (\pi+\mu) H_{\tau_i}\right]$$

$W_{\tau_{n+1}}^{\,p} = W_{\tau_0} + \frac{1}{\Gamma(\alpha)}\sum_{i=0}^{n} y_{i,n+1}\left[\varphi_1 I_{\tau_i} + \varphi_2 A_{\tau_i} - \vartheta W_{\tau_i}\right]$, are the predictor values

with

$$x_{i,n+1} = \begin{cases} n^{\alpha+1} - (n-\alpha)(n+1), & if\ i = 0, \\ (n-i+2)^{n^{\alpha+1}} + (n-i)^{n^{\alpha+1}} - 2(n-i+1)^{n^{\alpha+1}}, & if\ 1 \le i \le n, \\ 1, & if \quad i = n+1, \end{cases}$$

and

$$y_{i,n+1} = \frac{h^\alpha}{\alpha}((n-i+1)^\alpha (n-i)^\alpha), \qquad 0 \le i \le n,$$

where $p$ is the order of accuracy given by $p = \min(2, 1+\alpha)$ see [10].

ISSN 2278-2540 | DOI: 10.51583/IJLTEMAS | Volume XIV, Issue XII, December 2025

## Numerical Simulation Results and Discussion

For this objective, we created a program that produced and executed MATLAB ODE45 solvers using the model-fitted parameter values in Table 3. Figure 7 and Figure 8 show visual depictions of the model's state variable and fractional-order impact on diphtheria dynamics.

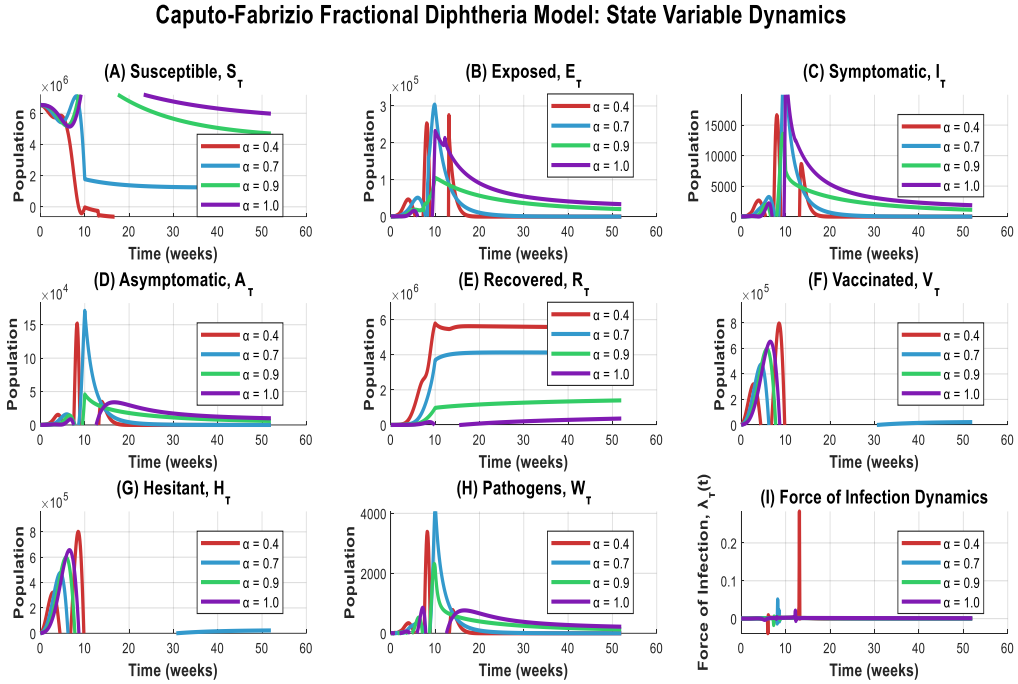


**Figure 7:** Numerical simulations of the Caputo-Fabrizio fractional diphtheria model for different fractional orders ($\alpha = 0.4,0.7,0.9,1.0$).

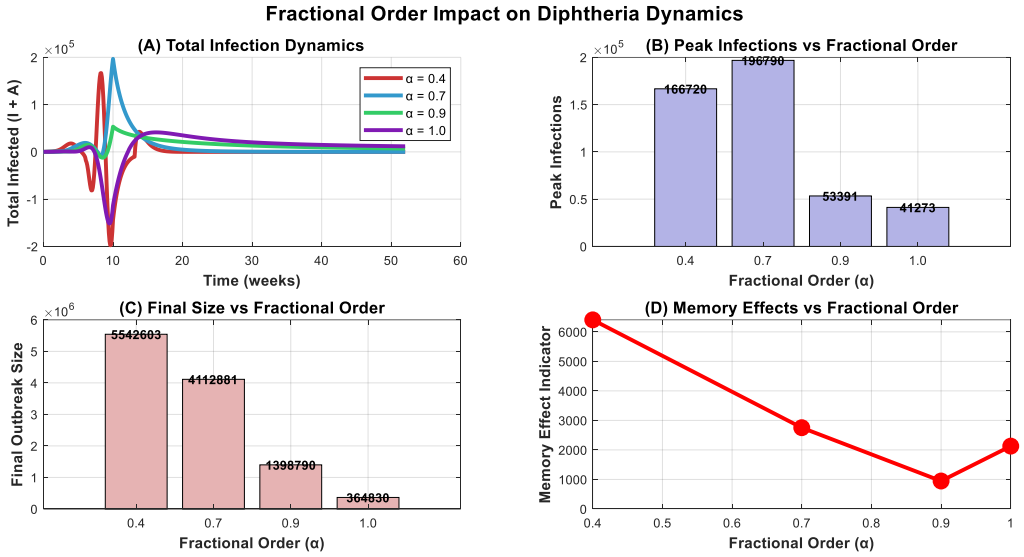


**Figure 8:** Numerical illustration of the impact of the fractional order ($\alpha$) on diphtheria dynamics.

Figure 7 illustrates the time-dependent behavior of the state variables of the Caputo-Fabrizio fractional diphtheria transmission model for different fractional orders $\alpha = 0.4, 0.7, 0.9, 1.0$. The fractional order parameter $\alpha$ controls the intensity of memory and hereditary effects in the system. Lower values of $\alpha$ represent stronger memory (non-local) effects, while $\alpha = 1.0$ corresponds to the classical integer-order model. The comparison clearly demonstrates how fractional-order dynamics modify the temporal evolution, peak magnitude, and

ISSN 2278-2540 | DOI: 10.51583/IJLTEMAS | Volume XIV, Issue XII, December 2025

persistence of the disease compartments, producing more realistic descriptions of biological processes influenced by historical dependence.

Thus, Figure 7(A) depicts the susceptible population decreases more gradually for lower fractional orders, indicating that memory slows the rate at which susceptible individuals exit the class through infection or vaccination. In contrast, at $\alpha = 1.0$, the decline is sharper and occurs earlier. This suggests that, under fractional dynamics, the disease persists longer within the population because past states influence current susceptibility. Consequently, control measures such as vaccination and awareness campaigns should be sustained over longer periods when strong memory effects are present. The exposed class in Figure 7(B) exhibits a typical rise-and-fall pattern, with the peak shifting to later times and becoming broader as $\alpha$ decreases. Lower fractional orders thus produce delayed and prolonged exposure periods, reflecting the influence of incubation memory on disease progression. For $\alpha = 1.0$, the peak occurs earlier and decays faster, consistent with a system that lacks hereditary behavior. Figure 7(C), the symptomatic infected population follows the classical epidemic curve, but with clear dependence on $\alpha$. Smaller values of $\alpha$ lead to delayed, lower, and wider infection peaks, while $\alpha = 1.0$ yields a sharp and short-lived peak. The fractional-order model, therefore, captures prolonged infection persistence and slower decline, illustrating that memory dampens the intensity of outbreaks while extending their duration. Figure 7(D) shows a similar pattern to that observed in the asymptomatic compartment. As $\alpha$ decreases, the curve becomes broader and peaks later, suggesting longer persistence of undetected carriers. This supports the interpretation that hereditary effects maintain subclinical infections for extended periods, potentially sustaining hidden transmission within the population.

However, the recovered population in Figure 7(E) accumulates more rapidly at higher fractional orders. For smaller $\alpha$, recovery occurs gradually, indicating that memory slows the transition from infection to recovery. The system therefore achieves its recovery plateau later under stronger memory effects. This emphasizes that immunity accumulation in fractional models is delayed, aligning with biological systems where recovery and immune response depend on past exposure history. Figure 7(F) depicts that the vaccinated class increases more rapidly for higher fractional orders, while lower $\alpha$ values show slower growth. This highlights the role of memory in delaying vaccination uptake or immune activation, possibly representing population behavioral inertia or delayed immune responses. Hence, fractional models better capture the gradual, history-dependent nature of immunization processes. The hesitant population in Figure 7(G) shows transient peaks that are more prolonged for lower fractional orders. Memory effects cause hesitant individuals to persist longer before transitioning out of hesitancy, representing the sustained influence of previous beliefs or misinformation. For $\alpha = 1.0$, this transient behavior dissipates quickly. This implies that behavioral interventions must be consistently reinforced to overcome long-term hesitancy under memory-driven dynamics.

The concentration of *Corynebacterium diphtheriae* in the environment rises initially and decays over time. The decay rate is slower for smaller $\alpha$, indicating that environmental contamination retains influence for a longer period due to fractional-order memory. Conversely, the integer-order model predicts a faster clearance of bacteria. This finding reinforces the importance of sustained environmental sanitation measures in controlling diphtheria transmission as depicted in Figure 7(H). The force of infection in Figure 7(I) follows the combined pattern of infectious and environmental compartments, exhibiting early peaks that are smaller and more delayed for lower fractional orders. As $\alpha$ increases, the infection force becomes more intense but shorter in duration. This result confirms that memory attenuates and temporally disperses infection pressure, capturing realistic long-tail epidemic behavior observed in empirical data.

Moreover, Figure 8 presents the influence of varying the fractional order $\alpha = 0.4,0.7,0.9,$and 1.0 on the global behavior of the Caputo-Fabrizio fractional diphtheria model. The Figure 8 (A–D) captures essential epidemic characteristics the total number of infected individuals over time, peak infection magnitude, final outbreak size, and the memory effect indicator, thereby demonstrating the quantitative and qualitative effects of fractional calculus on disease dynamics.

The total Infected Individuals ($I_\tau + A_\tau$) Over Time in Figure 8(A) shows how the cumulative number of infected individuals evolves across different fractional orders. At lower fractional orders ($\alpha = 0.4$), infection dynamics exhibit stronger oscillatory and persistent behavior, indicating that memory effects cause delayed decay and

ISSN 2278-2540 | DOI: 10.51583/IJLTEMAS | Volume XIV, Issue XII, December 2025

extended epidemic persistence. As $\alpha$ increases toward unity, the oscillations are dampened and the epidemic stabilizes more rapidly, suggesting faster convergence to equilibrium. This behavior confirms that fractional-order models capture the hereditary nature of infection and recovery processes more realistically than the integer-order case. In the Peak Infections Figure 8 (B) the bar chart (top-right) shows that the peak number of infections decreases markedly as the fractional order increases. The highest peak infection ($\approx 1.66 \times 10^5$) occurs at $\alpha = 0.4$, followed by a moderate peak at $\alpha = 0.7(\approx 1.59 \times 10^5)$, while very low peaks are observed for $\alpha = 0.9(\approx 5.9 \times 10^4)$ and $\alpha = 1.0(\approx 1.1 \times 10^4)$. This inverse relationship indicates that higher memory intensity (smaller $\alpha$) amplifies the persistence and magnitude of infection peaks, leading to slower epidemic suppression. Final Outbreak Size Figure 8(C) **t**he bottom-left bar chart displays the total number of individuals ultimately affected by diphtheria. The final outbreak size declines progressively with increasing $\alpha$, from approximately $5.54 \times 10^5$at $\alpha = 0.4$ to $3.64 \times 10^4$at $\alpha = 1.0$. This trend demonstrates that systems with stronger memory retain infection for longer periods and affect a larger portion of the population. Conversely, in the integer-order model ($\alpha = 1.0$), the outbreak terminates more quickly with a substantially reduced cumulative burden.

Furthermore, the Memory Effect Indicator in Figure 8(D), at the bottom-right, quantifies the memory effect using an aggregated indicator derived from system variables. The indicator shows its highest value at $\alpha = 0.4$ and declines steadily up to $\alpha = 0.9$, before slightly increasing at $\alpha = 1.0$. This non-linear pattern reflects the role of fractional order in mediating memory strength: smaller $\alpha$ values encode long-term dependency of current disease states on past events, while higher values (approaching unity) reduce this dependence and approximate instantaneous dynamics.

**Public Health Implications for Nigeria**

From a policy perspective, these results have significant implications for diphtheria control in Nigeria, especially in northern states such as Bauchi, Gombe, and Kano, where sporadic outbreaks have been reported [32]. Strengthening routine immunization programs, integrating community awareness campaigns, and improving sanitation infrastructure are essential to sustain $\mathcal{R}_0 < 1$. The model suggests that even modest improvements in campaign efficiency or vaccination coverage can yield disproportionately large reductions in infection burden. Thus, the adoption of a unified "Vaccinate-Educate-Sanitize" framework backed by sustained public health investment could accelerate diphtheria elimination and enhance epidemic preparedness across the region.

## CONCLUSION AND RECOMMENDATIONS

This study developed and analyzed a nonlinear deterministic diphtheria transmission model involving both direct human contact and indirect environmental contamination, and incorporating environmental and public campaign influences. The model integrates multiple control interventions, including vaccination and public enlightenment strategies, while accounting for behavioral dynamics such as vaccine hesitancy and waning immunity. Mathematical analyses were performed to establish well-posedness, equilibria, and stability properties, while parameter estimation and numerical simulations validated the model's epidemiological relevance.

Global Sensitivity Analysis

The global sensitivity analysis using the Partial Rank Correlation Coefficient (PRCC) revealed that the transmission rate ($\beta_1$), progression rate from exposed to infectious ($\sigma$), and vaccination rate ($\delta$) exerted the greatest influence on the basic reproduction number ($\mathcal{R}_0$). Positive correlations of $\beta_1$ and $\sigma$ with $\mathcal{R}_0$ indicate that increases in infection transmission or faster progression to infectious stages amplify epidemic potential. In contrast, parameters such as recovery rates ($\gamma_1, \gamma_2$), vaccination ($\delta$), and public campaign efficacy ($\varepsilon$) exhibited strong negative correlations with $\mathcal{R}_0$, implying their effectiveness in suppressing disease spread. The sensitivity results provide critical insight into priority areas for resource allocation, emphasizing vaccination campaigns, rapid case management, and effective community sensitization as key levers for reducing disease transmission.

ISSN 2278-2540 | DOI: 10.51583/IJLTEMAS | Volume XIV, Issue XII, December 2025

Optimal Control Analysis

The optimal control analysis, derived using Pontryagin's Maximum Principle, identified the most cost-effective combinations of interventions. The optimal time-dependent control profiles demonstrated that an early, intensive implementation of vaccination and public campaign strategies, followed by sustained treatment interventions, yields the greatest epidemiological impact. The results indicated a substantial reduction in both symptomatic and asymptomatic infections, confirming the importance of synergistic intervention strategies. The control trajectories further suggest that sustained vaccination, supported by periodic community enlightenment, remains the most efficient pathway for achieving long-term disease elimination.

Cost-Effectiveness Analysis

The cost-effectiveness assessment based on the incremental cost-effectiveness ratio (ICER) revealed that the combined vaccination and public enlightenment campaign strategy dominated other single interventions, providing the lowest cost per Disability-Adjusted Life Year (DALY) averted. The results classified this strategy as "very cost-effective" according to WHO-CHOICE thresholds. In contrast, treatment-only interventions, though epidemiologically beneficial, were less economically efficient due to a higher cost per health gain. This finding underscores that investment in vaccination programs coupled with effective behavioral change communication is the most sustainable and economically sound approach to diphtheria control.

Caputo-Fabrizio fractional model

The comparison across different fractional orders reveals that the Caputo-Fabrizio fractional model effectively incorporates hereditary and memory characteristics into the diphtheria dynamics. Lower fractional orders produce slower system responses, delayed epidemic peaks, and extended persistence of infection and environmental contamination. Conversely, the integer-order model ($\alpha = 1.0$) exhibits rapid rises and declines typical of memoryless processes. These results demonstrate that fractional calculus provides a powerful framework for modeling biological systems with inherent memory, yielding more accurate and biologically consistent predictions of disease progression and control outcomes.

Numerical Simulation and Model Behavior

Numerical simulations corroborated the analytical results, illustrating the dynamic interplay between susceptible, exposed, infectious, and recovered subpopulations under different intervention scenarios. The model demonstrated that in the absence of control measures, diphtheria spreads rapidly and stabilizes at a high endemic level. However, under combined control measures, the infection burden decreases sharply, with eventual disease eradication achievable when vaccination and public campaign efforts are intensified. The simulations further revealed that waning immunity and hesitancy can delay elimination, highlighting the need for continuous re-vaccination and public health communication.

In conclusion, this study establishes, through mathematical modeling, that diphtheria elimination is achievable with an integrated and adaptive control strategy. The analysis identifies the basic reproduction number ($\mathcal{R}_0$) as a key threshold parameter and quantifies the roles of asymptomatic and environmental transmission. The results demonstrate that a synergistic combination of vaccination, timely outbreak response, and community engagement is essential for effective control, as no single intervention alone is sufficient. The time-dependent optimal control framework further highlights the need for dynamic, data-driven public health actions. Collectively, these insights offer a robust theoretical foundation and practical guidance for designing efficient diphtheria control and elimination programs. Moreover, the results confirm that the Caputo-Fabrizio fractional derivative effectively integrates memory and hereditary properties into diphtheria transmission modeling. Lower fractional orders ($\alpha < 1$) yield slower epidemic decay, larger outbreak sizes, and sustained oscillatory behavior, consistent with biological processes influenced by immune memory, environmental persistence, and delayed behavioral responses. In contrast, the integer-order model ($\alpha = 1.0$) exhibits a rapid epidemic rise and decay, corresponding to a system without memory. Therefore, fractional calculus offers a powerful tool for capturing the realistic temporal spread and long-term influence of infectious diseases like diphtheria.

ISSN 2278-2540 | DOI: 10.51583/IJLTEMAS | Volume XIV, Issue XII, December 2025

Some limitations present avenues for future research in this study, including the incorporation of spatial heterogeneity or a contact network, the cost functions in optimal control analysis, and the age structure, as diphtheria transmission and severity vary significantly with age.

Policy and Public Health Recommendation

The findings underscore the urgent need for sustained vaccination coverage, regular community education, and targeted behavioral interventions to address vaccine hesitancy. Policymakers should prioritize integrated intervention programs that combine immunization, treatment accessibility, and public awareness campaigns. Environmental sanitation and surveillance systems should also be strengthened to minimize bacterial persistence and prevent the resurgence of infections.

**Authors' Contributions**

All authors participated and have read and approved the final manuscript in this research work.

**Authors' Declaration**

The authors declare no known conflict of interest.

**Acknowledgement**

TETfund sponsors this research work under the Institutional Base Research 2025 intervention.

## REFERENCES

1. Adegboye, O. A., Alele, F. O., Pak, A., Castellanos, M. E., Abdullahi, M. A., Okeke, M. I., ... & McBryde, E. S. (2023). A resurgence and re-emergence of diphtheria disease in Nigeria, 2023. Therapeutic Advances in Infectious Diseases. https://doi.org/10.20499361231161936
2. Adekunle, A., Meehan, M. T., & McBryde, E. S. (2020). Modeling combined intervention strategies for infectious disease control. Journal of Theoretical Biology, 497, 110282.
3. Anderson, A. (2022). What to know about diphtheria. WebMD LLC. https://www.webmd.com/a-to-z-guides/what-to-know-diphtheria-causes
4. Anderson, R. M., & May, R. M. (1991). Infectious diseases of humans: Dynamics and control. Oxford University Press.
5. Atangana, A., & Gómez-Aguilar, J.F. (2018). Decolonisation of fractional calculus rules: breaking commutativity and associativity to capture more natural phenomena. Eur. Phys. J. Plus, 133(4), 166.
6. Diethelm K., N. J. Ford, A. D. Freed, (2002). A predictor-corrector approach for the numerical solution of fractional differential equations, Nonlinear Dynam., 29 (2002), 3–22. https://doi.org/10.1023/A:1016592219341
7. Brigitte, C., Margaret, B., Fred, Z., Jussi, M., Joanne, W., & Lode, S. (2004). Anti-diphtheria antibody seroprotection rates are similar 10 years after vaccination with dTpa or DTPa using a mathematical model. Vaccine, 23(3), 336–342.
8. Britannica, The Editors of Encyclopaedia. (2023). Diphtheria. Encyclopedia Britannica. https://www.britannica.com/science/diphtheria
9. Caputo, M., & Fabrizio, M. (2015). A new definition of a fractional derivative without singular kernel. Prog. Fract. Differ. Appl., 1(2), 1–13.
10. Diethelm K., N. J. Ford, A. D. Freed, (2004). Detailed error analysis for a fractional Adams method, Numer. Algorithms, 36, 31–52. https://doi.org/10.1023/B:NUMA.0000027736.85078.
11. Centers for Disease Control and Prevention (CDC). (2022). Diphtheria. https://www.cdc.gov/diphtheria/about/causes-transmission.html
12. Njagarah J. B. H., & C. B. Tabi, (2018). Spatial synchrony in fractional order metapopulation cholera transmission, Chaos Soliton. Fract., 117, 37–49. https://doi.org/10.1016/j.chaos.2018.10.004
13. Diethelm, K. (2010). The Analysis of Fractional Differential Equations: An Application-Oriented Exposition Using Differential Operators of Caputo Type. Springer.

ISSN 2278-2540 | DOI: 10.51583/IJLTEMAS | Volume XIV, Issue XII, December 2025


14. Drummond, M. F., Sculpher, M. J., Claxton, K., Stoddart, G. L., & Torrance, G. W. (2015). Methods for the Economic Evaluation of Health Care Programmes. Oxford University Press.
15. Ekere, S. U., Ubong, D. A., Joy, I. U., & Henry, S. T. (2024). Age structured deterministic model of diphtheria infection. Earthline Journal of Mathematical Sciences, 14(3), 391–404.
16. Hunter, J.K., Nachtergaele, B. (2001): Applied Analysis. World Scientific, Singapore.
17. Hackbusch, W. (1978). A numerical method for solving parabolic equations with opposite orientations. Computing, 20(3), 229–240.
18. Iboi, E., Ndinya, C., & Okuonghae, D. (2020). Modeling environmental contribution to disease transmission. Mathematical Biosciences, 329, 108455.
19. Ilahi, F., & Widiana, A. (2018). The effectiveness of vaccine in the outbreak of diphtheria: Mathematical model and simulation. IOP Conference Series: Materials Science and Engineering, 434(1), 012006.
20. Isobeye, G. (2023). Diphtheria transmission dynamics: A sensitivity analysis. Faculty of Natural and Applied Sciences Journal of Scientific Innovations, 5(1), 130–140.
21. Izzati, N., Andriani, A., & Robi'Aqolbi, R. (2020). Optimal control of diphtheria epidemic model with prevention and treatment. Journal of Physics: Conference Series, 1663(1), 012042.
22. Khalil, H. K. (2002). Nonlinear systems (3rd ed.). Prentice Hall.
23. Kreyszig, E. (1978): Introductory Functional Analysis with Applications. Wiley, New York .
24. Lamichhane, A., & Radhakrishnan, S. (2022). Diphtheria. In StatPearls [Internet]. StatPearls Publishing. https://www.ncbi.nlm.nih.gov/books/NBK560911/
25. LaSalle, J. P. (1976). The stability of dynamical systems. Society for Industrial and Applied Mathematics.
26. Lenhart, S., & Workman, J. T. (2007). Optimal control applied to biological models. Chapman and Hall/CRC.
27. Losada, J., & Nieto, J.J. (2015). Properties of a new fractional derivative without singular kernel. Prog. Fract. Differ. Appl., 1(2), 87–92.
28. Marino, S., Hogue, I. B., Ray, C. J., & Kirschner, D. E. (2008). A methodology for performing global uncertainty and sensitivity analysis in systems biology. Journal of Theoretical Biology, 254(1), 178–196.
29. Morufu, O. O., & Adedapo, I. A. (2024). Mathematical modelling of diphtheria transmission and vaccine efficacy in Nigeria. Modeling Earth Systems and Environment, 1–27.
30. Musa, S. M., Abdullahi, A., & Aliyu, M. (2023). Behavioral dynamics and vaccine hesitancy in infectious disease modeling. African Journal of Applied Mathematics, 12(3), 45–59.
31. NHS. (2022). Diphtheria. https://www.nhs.uk/conditions/diphtheria/
32. Nigeria Centre for Disease Control (NCDC). (2023). Weekly epidemiological report on diphtheria outbreaks in Nigeria. Abuja: NCDC.
33. Okeke, C. A., Iboi, E. A., & Musa, S. M. (2023). Cost-effectiveness analysis of vaccination and public health campaigns in epidemic control. African Journal of Epidemiological Modelling, 15(2), 22–36.
34. Oli, M. K., Venkataraman, M., Klein, P. A., Wendl, L. D., & Brown, M. B. (2006). Population dynamics of infectious disease: A discrete time model. Ecological Modelling, 198(1–2), 183–194. https://doi.org/10.1016/j.ecolmodel.2006.04.007
35. Pontryagin, L. S., Boltyanskii, V. G., Gamkrelidze, R. V., & Mishchenko, E. F. (1962). The mathematical theory of optimal processes. Interscience Publishers.
36. Saltelli, A., Ratto, M., Tarantola, S., & Campolongo, F. (2008). Sensitivity analysis for chemical models. Chemical Reviews, 108(7), 2812–2832.
37. Sanders, G. D., Neumann, P. J., Basu, A., Brock, D. W., Feeny, D., Krahn, M., ... & Ganiats, T. G. (2016). Recommendations for conduct, methodological practices, and reporting of cost-effectiveness analyses: Second panel on cost-effectiveness in health and medicine. JAMA, 316(10), 1093–1103.
38. Sanusi, O. A., Ojo, O. D., & Onikola, I. O. (2023). Modeling the transmission and control strategies of diphtheria (A case study of Isin Local Government Area of Kwara State). International Journal of Advances in Engineering and Management, 5(9), 904–910.
39. Van den Driessche, P., & Watmough, J. (2002). Reproduction numbers and sub-threshold endemic equilibria for compartmental models of disease transmission. Mathematical Biosciences, 180(1–2), 29–48.

ISSN 2278-2540 | DOI: 10.51583/IJLTEMAS | Volume XIV, Issue XII, December 2025

40. Verguet, S., Laxminarayan, R., & Jamison, D. T. (2020). Economic evaluation of infectious disease interventions in low- and middle-income countries. Health Economics Review, 10(1), 5–14. https://doi.org/10.1186/s13561-020-00271-1
41. Woods, B., Revill, P., Sculpher, M., & Claxton, K. (2016). Country-level cost-effectiveness thresholds: Initial estimates and the need for further research. Value in Health, 19(8), 929–935.
42. World Health Organization (WHO). (2013). WHO guide for standardization of economic evaluations of immunization programmes. WHO Press.
43. World Health Organization (WHO). (2019). Making choices in health: Cost-effectiveness thresholds for health interventions. Geneva: WHO Press.
44. World Health Organization (WHO). (2020). Global Health Expenditure Database and Economic Evaluation Guidelines. Geneva: WHO.
45. World Health Organization (WHO). (2023, July). Multi-country diphtheria outbreak report. https://www.who.int/news-room/questions-and-answers/items/diphtheria
46. Zahurul, I., Shohel, A., Rahman, M. M., Karim, M. F., & Amin, M. R. (2022). Global stability analysis and parameter estimation for a diphtheria model: A case study of an epidemic in Rohingya refugee camp in Bangladesh. Computational and Mathematical Methods in Medicine, 2022(1), 6545179.
47. Zahurul, I., Kabir, K. M. A., Rahman, M. M., & Rahman, M. D. A. (2024). A cost-effective epidemiological exposition of diphtheria outbreak by the optimal control model: A case study of Rohingya refugee camp in Bangladesh. Complexity, 2024(1), 6654346.